American Mineralogist, Volume 89, pages 614–628, 2004

Model pyroxenes II: Structural variation as a function of tetrahedral rotation

RICHARD M. THOMPSON* AND ROBERT T. DOWNS

Department of Geosciences, University of Arizona, Tucson, Arizona 85721-0077, U.S.A.

ABSTRACT

Model pyroxenes with regular tetrahedral and M1 octahedral coordination polyhedra have been derived. The M2 polyhedron is not constrained to be regular. These models are parameterized in terms of the O3-O3-O3 angle, θ, and the model O atom radius, *r*. Crystallographic parameters such as interatomic distances, unit cell volume, and packing distortion are determined as a function of the O3-O3-O3 angle. Results are compared with observed pyroxenes, providing insight into which interatomic interactions are important in determining pyroxene topology and behavior. Temperature is shown to favor polyhedral regularity in orthopyroxene and protopyroxene. Compression and expansion strain ellipsoids for observed and model pyroxenes are compared, demonstrating that a combination of tetrahedral rotation and isotropic compression approximately reproduces the compression ellipsoids of pyroxenes, but not the expansion ellipsoids.

INTRODUCTION

The term pyroxene refers to a group of crystal structures that include important components of the Earth's crust and mantle, lunar and Martian rocks, and meteorites (Deer et al. 1978). Many pyroxene phases not found in nature have been synthesized. There are several naturally occurring polymorphs, commonly displaying $P2_1/c$, $C2/c$, *Pbcn*, or *Pbca* symmetry. More rarely, cation ordering on a given site results in $P2/n$ symmetry. These have been described in detail by Cameron and Papike (1981), and at pressure and temperature by Yang and Prewitt (2000).

Two of the defining structural elements in pyroxenes are chains of edge-sharing octahedra and corner-sharing tetrahedra that run parallel to **c** (Fig. 1). The cation sites in a given chain are related to each other by a **c**-glide perpendicular to **b**. The octahedral cation sites are called M1. There are additional cation sites called M2 tucked into the kinks of the octahedral chain (M2 is not shown in Fig. 1). The O anions on the shared edges of the octahedra are called O1; these O atoms are also coordinated to T. The O atoms shared between tetrahedra are called O3. The remaining O atoms share coordination with T, M1, and M2, and are called O2.

The anion skeletons of some pyroxenes have long been described as distorted closest-packed arrangements (cf. Peacor 1968; Thompson 1970; Papike et al. 1973). Thompson and Downs (2003) derived crystal structure parameters for all possible ideal pyroxenes based on closest-packed stacking sequences of length 12 or less. They established a correspondence between the different observed topologies and some of the ideal pyroxenes. Their work shows that observed pyroxene polymorphs have the smallest possible numbers of crystallographically distinct polyhedra.

Thompson and Downs (2003) also showed that M-T distances determine hypothetical relative energies of ideal pyroxenes. Every ideal pyroxene can be thought of as being constructed from portions of CCP and HCP pyroxene. One of the M2-T distances in an HCP portion is 28% shorter than the equivalent M2-T distance in a CCP portion, while one of the HCP M1-T distances is 11% longer than its CCP equivalent. Thompson and Downs (2003) suggested that these M-T repulsions are important factors determining the topologies of observed pyroxenes.

Observed pyroxene topologies are often characterized by the geometry of their tetrahedral chains and the orientation of those tetrahedral chains relative to their "associated" octahedral chains (cf. Thompson 1970; Papike et al. 1973; Arlt and Angel 2000b; Tribaudino et al. 2002). Tetrahedral and octahedral chains are said to be "associated" if they share O1, as illustrated in Figure 1. The structural parameter commonly used to describe this geometrical arrangement is the O3-O3-O3 angle.

The O3-O3-O3 angle has traditionally been described in terms of tetrahedral rotation away from a model value of 180° (Thompson 1970; Papike et al. 1973). This hypothetical rotation is about an axis parallel to **a*** passing through O1 and T. A tetrahedral chain with an O3-O3-O3 angle greater than 180° has traditionally been referred to as S-rotated; if the O3-O3-O3 angle is less than 180°, then the traditional notation is O-rotated (Thompson 1970). An idealized pyroxene with regular octahedra and tetrahedra and a "completely rotated" O3-O3-O3 angle of 120° is cubic closest-packed, while an ideal pyroxene with an O3-O3-O3 angle of 240° is hexagonal closest-packed (Thompson 1970; Papike et al. 1973). The M2 site in these two idealized extremes is centered in a perfect octahedron. Observed pyroxenes have O3-O3-O3 angles that lie between these extremes.

Real pyroxenes can be quite distorted from their ideal equivalents. For instance, ideal orthopyroxene has space group $P2_1ca$ and eight crystallographically distinct polyhedra, while observed orthopyroxene has space group *Pbca* and four distinct polyhedra (Thompson and Downs 2003). Most clinopyroxenes, while retaining the space groups of their ideal equivalents, have O3-O3-O3 angles quite different from ideal values. For example,

* E-mail: Thompson@geo.arizona.edu

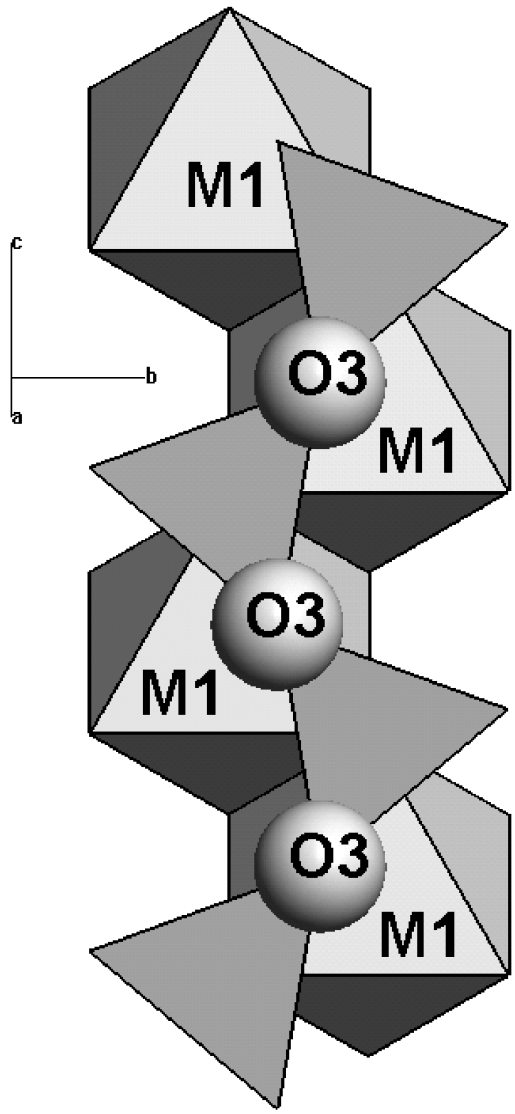

FIGURE 1. Portion of a model pyroxene with O3-O3-O3 angle = 160°. This angle is commonly used to characterize pyroxene topologies. If the angle formed by the three O3 atoms and the angle formed by the M1 atoms with approximately the same *z*-coordinates are concave in the same direction, then O3-O3-O3 < 180° (O-rotated). If these angles are concave in opposite directions, then O3-O3-O3 > 180° (S-rotated).

$LiFeSi_2O_6$ displays an O3-O3-O3 angle of 180.83°, almost exactly half way between the ideal values of 120° (CCP) and 240° (HCP) (Redhammer et al. 2001). The significant departure of the observed O3-O3-O3 angle from ideal values motivates the search for more realistic models of pyroxenes that have anion arrangements that are not constrained by closest-packing.

Pannhorst (1979, 1981) made models of pyroxenes that include tetrahedral chains with an O3-O3-O3 angle of 180°, but did not derive crystal structure parameters. The basic structural unit in his model is a layer of O atoms parallel to (100) and some of the adjacent cations. He named three different layer types: M'K, MK, and MS. He derived rules describing how these units can be stacked and then presented the possible polymorphs in terms of these units and compared his models to observed pyroxenes.

Chisholm (1981, 1982) made models of pyroxenes that place no constraints on the O3-O3-O3 angle. The basic structural unit is the so-called "I-beam" (Papike and Ross 1970), an octahedral chain and its associated tetrahedral chains (a tetrahedral chain has only one associated octahedral chain, but an octahedral chain has two associated tetrahedral chains, one above it in the **a*** direction, and one below it.) In Chisholm's model (1981, 1982), structures are constrained to have no more than two types of tetrahedral layers, and no tetrahedral layer may contain more than one type of tetrahedral chain. He derived space groups for all of the possible structures generated by his model, showing that it generates all of the commonly observed polymorphs.

The models of Pannhorst (1979, 1981) and Chisholm (1981, 1982) do not include crystal structure data and therefore cannot be used to make quantitative comparisons between the models and observed pyroxenes. Thompson and Downs (2003) provide crystal structures for ideal pyroxenes, but the values of the O3-O3-O3 angles in many observed pyroxenes are extremely distorted from the closest-packed values of 120° and 240°, limiting the conclusions that can be drawn from comparison of ideal and observed pyroxenes. We are therefore motivated to search for a reasonable model that will allow the calculation of M-T distances and other crystallographic parameters as a function of O3-O3-O3 angle. Analysis of such a model may give additional insight into which crystallographic parameters control observed topologies and how they do so.

Comparing the bonding and packing of ideal and observed *C*2/*c* pyroxenes reveals another limitation of the closest-packing model. In some cases, the bonding topology (Downs 2003) resembles the ideal HCP pyroxene, but the O atom packing more closely resembles CCP. For instance, electron density analysis of kosmochlor shows that it has the bonding topology of an ideal HCP pyroxene, but its O atom packing more closely resembles CCP and moves toward CCP with pressure (Origlieri et al. 2003). Analysis of a model that allows tetrahedral rotation may reconcile these apparent inconsistencies.

In this paper, we derive crystal structures for model clinopyroxenes, orthopyroxene, protopyroxene, $P2_1ca$ theoretical high-*P* orthopyroxene, and $P2_1cn$ high-*P* protopyroxene, all with variable O3-O3-O3 angles. In these models, the M1 and T polyhedra are regular and the tetrahedral volume is fixed with tetrahedral edge = 2*r*, where *r* is the model O atom radius. In some of these structures, there is more than one nonequivalent tetrahedral chain and O3-O3-O3 angle. In this case, the TA volume is fixed.

We have used the simple constraints of regular M1 and T polyhedra to derive formulae for the structural parameters of our models in terms of the O3-O3-O3 angle and *r*. Thus, we can solve for any crystallographic parameters that are derived from crystal structure data as a function of the O3-O3-O3 angle, such as interatomic distances and unit cell volume. Furthermore, we can model any observed pyroxene by setting the model O3-O3-O3 angle and unit cell volume equal to the observed values.

CRYSTAL STRUCTURES OF THE MODELS

This section presents equations for the cell and positional parameters of our model pyroxenes in terms of the model O atom radius, *r*, and the O3-O3-O3 angle, which will be called θ in the remainder of this paper. Low clinopyroxene, orthopyroxene, and $P2_1cn$ high-*P* protopyroxene have two nonequivalent tetra-

hedral chains, and are parameterized in terms of θA, θB, and r, where r = half of the A-chain tetrahedral edge length, e_{TA}. $P2_1ca$ high-P orthopyroxene has four nonequivalent O3-O3-O3 angles so it is parameterized in terms of θA, θB, θC, θD, and r. The equations have been solved for various values of θ and the geometry of the resulting structures have been checked to verify that the constraints of the model are satisfied. The model $C2/c$ pyroxene is derived in the Appendix to illustrate the process.

Because θ has previously been quantified in several different ways, we need to define the standard used in this paper. Thompson and Downs (2003) presented a procedure for determining the value of θ when looking down **a*** at octahedral chains with negative tilt. The value of this angle is unambiguous for any chain in any pyroxene when the following procedure is used. Any two adjacent tetrahedra contain three O3 atoms. There are three M1 atoms in the associated octahedral chain that are immediately below the three O3 atoms when looking down **a*** (above the O3 atoms when looking up **–a***). If the angles formed by the O3 atoms and by the M1 atoms are concave in the same direction, then θ is less than 180°, otherwise it is greater than 180°. In Figure 1, θ is 160°.

Information relating to the different model pyroxenes is given in Table 1. The $P2_1/c$ model pyroxene results when alternating layers of tetrahedral chains in the $C2/c$ model pyroxene are allowed to have nonequivalent θ atoms.

In the *Pbca* model pyroxene, TA and M1 cannot both be regular unless θA = 180°. Figure 2 illustrates this. Both O2 and O1 must have the same z-coordinate if the octahedron is to be regular. O2' also has the same z-coordinate because it is related to O2 by a **b**-glide perpendicular to **a**. Thus, the O1-O2-O2' plane is perpendicular to **c**. The **O3-O3** vector must be perpendicular to this plane by the geometry of a tetrahedron, and so is parallel to **c**. This will be true of all the tetrahedra in the chain because of the **c**-glide, so all **O3-O3** vectors are parallel to **c**, and θA = 180°. Because of the relative position of the **b**-glide, this constraint does not hold for θB and polyhedral distortion is independent of θB.

As mentioned above, when θA ≠ 180°, M1 and TA cannot simultaneously be regular. Thus, two different orthopyroxene models can be constructed: one that has regular M1 and one that has regular TA. There are several ways to construct these models. We chose to let the placement of O1A determine which polyhedron will be regular. Thus, two equations for O1A are given below, one that makes TA regular, one that makes M1 regular.

The $P2_1ca$ model pyroxene is Thompson's (1970) "predicted inversion form" for orthopyroxene, i.e., its predicted high-P polymorph. It has four nonequivalent tetrahedra and two nonequivalent M1 octahedra. The four tetrahedra and two octahedra are regular if and only if 180° – θA = θB – 180° and θC = θD. Figure 3 illustrates this with a portion of the structure when θA = 120° and θB = 240°. The triangular outline is the base of an octahedron. If θA is fixed while θB decreases and the tetrahedra are kept regular, then either the octahedron above or below must distort. There are two equations presented below for TB, O1B, TD, and O1D. One set makes all the tetrahedra and M1b regular; the other makes TA, TC, and both M1 octahedra regular. The model orthopyroxene structure with space group *Pbca* and regular TA, TB, and M1 results when θA = θB = 180° and θC = θD.

In *Pbcn* model pyroxene, T and M1 cannot both be regular unless θ = 180°. As with the model orthopyroxene structure, this is a consequence of the **b**-glide.

$P2_1cn$ model pyroxene is Thompson's (1970) "predicted inversion form" for protopyroxene and a transition to this polymorph was observed by Yang et al. (1999). The model $P2_1cn$ structure has regular TA, TB, and M1 if and only if θA – 180° = 180° – θB. The model protopyroxene structure with space group *Pbcn* and regular T and M1 results when θA = θB = 180°.

Reasonability of the Models

Traditional measures of polyhedral distortion computed for observed pyroxenes show that the models successfully approximate observed structures. Robinson et al. (1971) presented definitions of two measures of polyhedral distortion, bond angle variance and quadratic elongation, and applied these to some common rock-forming minerals. The pyroxene polyhedra are among the least distorted of the minerals they analyzed.

Table 2 compares the angle variance and quadratic elongation for the M1 and T polyhedra in some observed pyroxenes at various conditions, and contrasts these with forsterite. Olivines have long been described as having nearly closest-packed O atom arrangements (cf. Megaw 1973) and Thompson and Downs (2001) demonstrated this quantitatively. Thus, olivine polyhedra should be relatively undistorted. Despite the fact that the bulk structural distortion of the pyroxene structure is greater than that of olivine, often by a factor of three or more (Thompson and Downs 2001), the M1 and T polyhedra in pyroxene are significantly less distorted than the octahedra and tetrahedra in forsterite. Thus, the distortion of the pyroxene structure results from distortion of the M2 polyhedra, not from M1 or T.

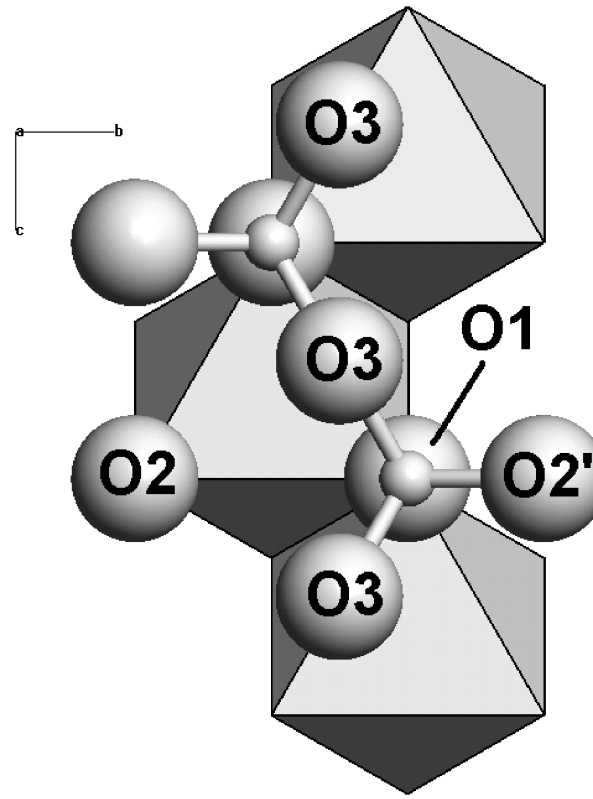

Figure 2. In model orthopyroxene, TA and M1 cannot both be regular unless O3A-O3A-O3A = 180°. Both O2 and O1 must have the same z-coordinate for the octahedron to be regular. O2' also has the same z-coordinate because it is related to O2 by a **b**-glide perpendicular to **a**. Thus, the O1-O2-O2' plane is perpendicular to **c**. The **O3-O3** vector must be perpendicular to this by the geometry of a tetrahedron, and so is parallel to **c**. This will be true of all the tetrahedra in the chain thanks to the **c**-glide, so all **O3-O3** vectors are parallel to **c**, and O3A-O3A-O3A = 180°.

If the model constraints reflect physically meaningful principles governing the topologies of real pyroxenes, then the tetrahedral chains in protopyroxenes and the TA chains in orthopyroxenes should be as straight as possible because T and M1 can both be regular only when θ = 180°. θ values for these chains are observed to lie in the range 158–180°. As pressure increases from 0 to 8.10 GPa in orthoenstatite (Hugh-Jones and Angel 1994), θB decreases from 139.00° to 136.43°. However, θA is essentially fixed (158.71° to 158.52°), despite the fact that decreasing θA would reduce volume (see below). The chain geometries in orthorhombic pyroxenes appear to be a compromise between maintaining polyhedral regularity and maximizing R(M2-T) (discussed in the introduction). Thus, the tendency to keep T and M1 regular is an important factor in determining the topology of the pyroxenes.

TABLE 1. Crystal structure data for models of the most common pyroxenes including their computational, cell, and positional parameters

	*C*2/*c* model pyroxene	$P2_1/c$ model pyroxene	*Pbca* model pyroxene
e_{M1}	$\sqrt{(8/3)}r\sqrt{(1 - \cos\theta)}$	$\sqrt{(8/3)}r\sqrt{(1 - \cos\theta A)}$	$\sqrt{(8/3)}r\sqrt{(1 - \cos\theta A)}$
e_{TB}		$2r\sqrt{[(1 - \cos\theta A)/(1 - \cos\theta B)]}$	$2r\sqrt{[(1 - \cos\theta A)/(1 - \cos\theta B)]}$
e_{TC}			
e_{TD}			
h_{TA}	$2\sqrt{6}r/3$	$2\sqrt{6}r/3$	$2\sqrt{6}r/3$
h_{TB}		$\sqrt{6}e_{TB}/3$	$\sqrt{6}e_{TB}/3$
h_{TC}			
h_{TD}			
h_{M1}	$\sqrt{6}e_{M1}/3$	$\sqrt{6}e_{M1}/3$	$\sqrt{6}e_{M1}/3$
d	$a\sin\beta = 2h_T + 2h_{M1}$	$a\sin\beta = h_{TA} + h_{TB} + 2h_{M1}$	
A	$-2r\cos(\theta/2)/\sqrt{3}$	$-r\cos(\theta A/2)/\sqrt{3}$	$2r\cos(\theta A/2)/\sqrt{3}$
B		$-(e_{TB}/2)\cos(\theta B/2)/\sqrt{3}$	$-(e_{TB}/2)\cos(\theta B/2)/\sqrt{3}$
C			
β	$90° + \tan^{-1}((e_{M1}/\sqrt{3} + A)/(d/2))$	$90° + \tan^{-1}((c/3 + A + B)/(d/2))$	
a	$d/\sin\beta$	$d/\sin\beta$	$2h_{TA} + 2h_{TB} + 4h_{M1}$
b	$3e_{M1}$	$3e_{M1}$	$3e_{M1}$
c	$\sqrt{3}e_{M1}$	$\sqrt{3}e_{M1}$	$\sqrt{3}e_{M1}$
M1a	[0 11/12 1/4]	$[(h_{TA}/2 + h_{M1}/2)/d, 2/3, 1/12 + (h_{TA}/2 + h_{M1}/2)\tan(\beta - 90°)/c - A/c]$	$[(h_{TA} + (1/2)h_{TB} + (3/2)h_{M1})/a, 2/3, z_{O2B} + 1/6]$
M1b			
M2a	[0 1/4 1/4]	$[x_{M1}, 0, z_{M1}]$	$[x_{M1}, 1/2, z_{M1} - 1/2]$
M2b			
TA	$[((3/4)h_T + h_{M1}/2)/d, 1/12, 5/12 - (h_T/4 + h_{M1}/2)\tan(\beta - 90°)/c + A/c]$	$[(h_{TA}/4)/d, 1/3, 1/4 + (h_{TA}/4)\tan(\beta - 90°)/c + A/c]$	$[((3/4)h_{TA} + (1/2)h_{TB} + h_{M1})/a, 1/3, z_{O2A} + A/c]$
TB		$[(h_{TA}/2 + (3/4)h_{TB} + h_{M1})/d, 5/6, 1/4 + (h_{TB}/4)\tan(\beta - 90°)/c + B/c]$	$[(h_{TA} + (3/4)h_{TB} + 2h_{M1})/a, 1/3, 3/4 - B/c]$
TC			
TD			
O1A	$[(h_{M1}/2)/d, 1/12, z_T - (3/4)h_T\tan(\beta - 90°)/c]$	$[-(h_{TA}/2)/d, 1/3, z_{TA} - (3/4)h_{TA}\tan(\beta - 90°)/c]$	$[(h_{TB}/2 + h_{M1})/a, 1/3, z_{TA}]$* $[(h_{TB}/2 + h_{M1})/a, 1/3, z_{O2A}]$†
O1B		$[(h_{TA}/2 + h_{M1})/d, 5/6, z_{TB} - (3/4)h_{TB}\tan(\beta - 90°)/c]$	$[(h_{TA} + (3/2)h_{TB} + 2h_{M1})/a, 1/3, z_{TB}]$
O1C			
O1D			
O2A	$[(h_T + h_{M1}/2)/d, 1/4, z_T + (h_T/4)\tan(\beta - 90°)/c - A/c]$	$[-x_{O1A}, 1/2, 1/2 - z_{TA} + (3/4)h_{TA}\tan(\beta - 90°)/c]$	$[(h_{TA} + (1/2)h_{TB} + h_{M1})/a, 1/2, z_{M1} + 1/6]$
O2B		$[x_{O1B} + h_{TB}/d, 0, 1/2 - z_{TB} + (3/4)h_{TB}\tan(\beta - 90°)/c]$	$[x_{O1B} - h_{TB}/a, 1/2, 3/4 + B/c]$
O2C			
O2D			
O3A	$[x_{O2}, r\cos(\theta/2)/b, z_{O2} + 1/2 + 2r\sin(\theta/2 - 60°)/c]$	$[x_{O2A}, 1/4 - r\cos(\theta A/2)/b, z_{O2A} + 1/2 + 2r\sin(\theta A/2 - 120°)/c]$	$[x_{O2A}, 1/4 - r\cos(\theta A/2)/b, z_{O2A} - 2r\sin(\theta A/2 - 60°)/c]$
O3B		$[x_{O2B}, 3/4 - (e_{TB}/2)\cos(\theta B/2)/b, z_{O2B} + 1/2 + e_{TB}\sin(\theta B/2 - 120°)/c]$	$[x_{O2B}, 1/4 - (e_{TB}/2)\cos(\theta B/2)/b, z_{O2B} - e_{TB}\sin(\theta B/2 - 60°)/c]$

Symbols for the computational parameters have the following meanings: θ is the O3-O3-O3 angle, *r* is the model oxygen radius = tetrahedral edge length (in the A-chain) / 2, *e* is the edge length of a polyhedron, *h* is the height, and A is a distance parallel to c associated with the A tetrahedral chain. * in a regular TA tetrahedra; † in a regular M1 octahedra; ‡ in a regular tetrahedron; § in a regular octahedron.

RESULTS

We call a model pyroxene "equivalent" to an observed structure if they both have the same θs and unit cell volumes. Every observed structure has a model equivalent, constructed by setting the model θ equal to the observed value, and adjusting *r* until the model cell volume equals the observed value. Structural data for the model equivalents of the observed pyroxenes listed in Table 2 and Table 8 are presented in Tables 3–7. Table 3 contains the data for model equivalents of 30 observed *C*2/*c* pyroxenes plus seven structures with θ ranging from 240° (HCP) to 120° (CCP) by 20° increments. Table 4 contains the data for the model equivalents of the low clinopyroxenes and two idealized structures. One idealized structure is closest-packed and has θA = 240°, θB = 120°, and is based on stacking sequence ABABCACABCBC (Thompson and Downs 2003). The other has θA = 180° and θB = 120°. Table 5 contains the data for the model equivalents of the orthopyroxenes and two idealized structures. One idealized structure has θA = 180° and θB = 120°; the other has θA = θB = 180°. Table 6 contains the data for the model equivalents of the protopyroxenes and the idealized protopyroxene with θ = 180°. Table 7 contains the data for the model equivalents of the two high-*P* protopyroxenes with space group $P2_1cn$ and for the closest-packed structure with θA = 120° and θB = 240° that is based on stacking sequence ABAC (Thompson and Downs 2003). The appendix contains exact structural data for some of the idealized structures.

ANALYSIS

Unit-cell volume

Model unit cell volume varies with θ when tetrahedral volume is fixed. The ratio of octahedral to tetrahedral edge length increases from 1 at θ = 120° to $2/\sqrt{3}$ = 1.15 at θ = 180° and decreases back to 1 at θ = 240° (Papike et al. 1973). Thus, octahedral volume and unit cell volume range from a minimum at θ = 120° and 240° to a maximum at θ = 180°.

TABLE 1—continued

	$P2_1ca$ model pyroxene	$Pbcn$ model pyroxene	$P2_1cn$ model pyroxene
e_{M1}	$\sqrt{(8/3)}r\sqrt{(1 - \cos\theta A)}$	$\sqrt{(8/3)}r\sqrt{(1 - \cos\theta)}$	$\sqrt{(8/3)}r\sqrt{(1 - \cos\theta A)}$
e_{TB}	$2r\sqrt{[(1 - \cos\theta A)/(1 - \cos\theta B)]}$		$2r\sqrt{[(1 - \cos\theta A)/(1 - \cos\theta B)]}$
e_{TC}	$2r\sqrt{[(1 - \cos\theta A)/(1 - \cos\theta C)]}$		
e_{TD}	$2r\sqrt{[(1 - \cos\theta A)/(1 - \cos\theta D)]}$		
h_{TA}	$2\sqrt{6}r/3$	$2\sqrt{6}r/3$	$2\sqrt{6}r/3$
h_{TB}	$\sqrt{6}e_{TB}/3$		$\sqrt{6}e_{TB}/3$
h_{TC}	$\sqrt{6}e_{TC}/3$		
h_{TD}	$\sqrt{6}e_{TD}/3$		
h_{M1}	$\sqrt{6}e_{M1}/3$	$\sqrt{6}e_{M1}/3$	$\sqrt{6}e_{M1}/3$
d			
A	$2r\cos(\theta A/2)/\sqrt{3}$		$-2r\cos(\theta A/2)/\sqrt{3}$
B			
C	$-e_{TC}\cos(\theta C/2)/\sqrt{3}$		
β			
a	$2h_{TA} + 2h_{TC} + 4h_{M1}$	$2h_T + 2h_{M1}$	$2h_{TA} + 2h_{M1}$
b	$3e_{M1}$	$3e_{M1}$	$3e_{M1}$
c	$\sqrt{3}e_{M1}$	$\sqrt{3}e_{M1}$	$\sqrt{3}e_{M1}$
M1a	$[x_{O2A} + (1/2)h_{M1}/a, 2/3, z_{O2A} + 1/3]$	[0 1/12 3/4]	$[0, 1/12, z_{O2B} + 2/3]$
M1b	$[x_{O1C} + (1/2)h_{M1}/a, 1/6, z_{TC} - 1/6]$		
M2a	$[x_{M1a}, 0, z_{M1a}]$	[0 1/4 1/4]	$[x_{M1}, 1/4, z_{M1} - 1/2]$
M2b	$[x_{M1b}, 1/2, z_{M1b}]$		
TA	$[((3/4)h_{TA} + (1/2)h_{TC} + h_{M1})/a, 1/6, 7/12 + (C + A)/(2c)]$	$[((3/4)h_T + h_{M1}/2)/a, 1/12, 1/12]$	$[((3/4)h_{TA} + h_{M1}/2)/a, 1/12, 1/12 + A/(2c)]$
TB	$[x_{O2B} + (1/4)h_{TB}/a, 2/3, z_{O2B} + (e_{TB}/\sqrt{3})\cos(\theta B/2)/c]$‡ $[x_{O2B} + (1/4)h_{TB}/a, 2/3, z_{O2A}]$§		$[(h_{TB}/4 + h_{M1}/2)/a, 7/12, z_{O2A}]$
TC	$[x_{O2C} + (1/4)h_{TC}/a, 1/3, z_{O2C} - C/c]$		
TD	$[x_{O2D} - (1/4)h_{TD}/a, 5/6, z_{O2D} - (e_{TD}/\sqrt{3})\cos(\theta D/2)/c]$‡ $[x_{O2D} - (1/4)h_{TD}/a, 5/6, z_{O2C}]$§		
O1A	$[x_{TA} - (3/4)h_{TA}/a, 1/6, z_{TA}]$	$[(h_{M1}/2)/a, 1/12, 1/12]$	$[(h_{M1}/2)/a, 1/12, z_{TA}]$
O1B	$[x_{O2B} + h_{TB}/a, 2/3, z_{TB}]$‡ $[x_{O2A}, 2/3, z_{TB}]$§		$[x_{TB} + (3/4)h_{TB}/a, 7/12, z_{TB}]$‡ $[x_{O2A}, 7/12, z_{TB}]$§
O1C	$[x_{O2C} + h_{TC}/a, 1/3, z_{TC}]$		
O1D	$[x_{O2D} - h_{TD}/a, 5/6, z_{TD}]$‡ $[x_{O2C}, 5/6, z_{TD}]$§		
O2A	$[x_{O1A} + h_{TA}/a, 0, z_{TA} - A/c]$	$[(h_T + h_{M1}/2)/a, 1/4, z_T + 2r\cos(\theta/2)/\sqrt{3}]$‡ $[(h_T + h_{M1}/2)/a, 1/4, z_T]$§	$[x_{O1A} + h_{TA}/a, 1/4, z_{TA} - A/c]$
O2B	$[x_{O1A}, 1/2, z_{O1A}]$		$[x_{O1A}, 3/4, z_{O1B} + (e_{TB}\cos(\theta B/2)/\sqrt{3})/c]$
O2C	$[x_{O2A} + h_{M1}/a, 1/2, z_{O2A} + 1/6]$		
O2D	$[x_{O1C}, 0, z_{O1C}]$		
O3A	$[x_{O2A}, 2r\cos(\theta A/2 - 60°)/b, z_{O2A} - 2r\sin(\theta A/2 - 60°)/c]$	$[x_{O2}, 1/4 - 2r\cos(\theta/2 - 60°)/b, z_{O2} + 2r\sin(\theta/2 - 60°)/c]$	$[x_{O2A}, y_{O2A} - 2r\cos(\theta A/2 - 60°)/b, z_{O2A} + 2r\sin(\theta A/2 - 60°)/c]$
O3B	$[x_{O2B}, 1/2 + e_{TB}\cos(120° - \theta B/2)/b, z_{O2B} + e_{TB}\sin(120° - \theta B/2)/c]$		$[x_{O2B}, y_{O2B} - e_{TB}\cos(120° - \theta B/2)/b, z_{O2B} - e_{TB}\sin(120° - \theta B/2)/c]$
O3C	$[x_{O2C}, e_{TC}\sin(\theta C/2 - 30°)/b, z_{O2C} - e_{TC}\sin(\theta C/2 - 60°)/c]$		
O3D	$[x_{O2D}, 1 - e_{TD}\cos(\theta D/2 - 60°)/b, z_{O2D} + e_{TD}\sin(\theta D/2 - 60°)/c]$		

Figure 4 illustrates the relationship between unit cell volume and θ for the model $C2/c$ pyroxene when $r = 1$. The equation is

$$V = (32\sqrt{2}(1 - \cos\theta) + 64(1 - \cos\theta)^{3/2}/\sqrt{3})r^3.$$

Figure 5 illustrates how unit-cell volume varies for the model $P2_1/c$ pyroxene as a function of θA and θB along a pathway in the (θA, θB) domain that represents an idealized phase transition sequence. The pathway begins with a fully extended (θ

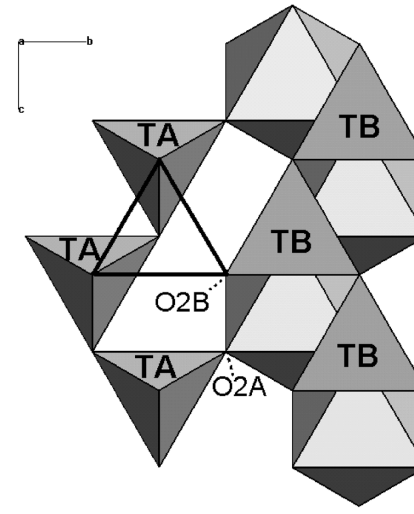

FIGURE 3. Model $P2_1ca$ theoretical high-pressure orthopyroxene only has all polyhedra regular if 180° – O3A-O3A-O3A = O3B-O3B-O3B – 180°. In this view, O3A-O3A-O3A = 120° and O3B-O3B-O3B = 240°. The triangular outline is the base of an octahedron. By inspection, if the above relation is not true (e.g., one chain rotates while the other remains fixed), then the octahedron cannot be regular.

TABLE 2. Bond angle variance, σ, and quadratic elongation, λ, for some pyroxenes at various conditions and forsterite

Mineral	Phase	Condition	σ_{TA}	λ_{TA}	σ_{TB}	λ_{TB}	σ_{M1}	λ_{M1}	Reference	Ref no.
diopside	8-CN M2 C2/c px	24 °C	28.54	1.007			17.38	1.005	Cameron et al. (1973)	1a
		1000 °C	27.96	1.007			20.00	1.006		1b
		5.3 GPa	28.30	1.007			17.58	1.005	Levien and Prewitt (1981)	2b
enstatite	low clinopyroxene	20 °C	31.85	1.008	18.88	1.005	25.98	1.009	Pannhorst (1984)	3a
		700 °C	33.04	1.008	19.73	1.005	28.93	1.010		3b
	orthopyroxene	296 K	38.97	1.010	19.60	1.005	26.24	1.009	Yang and Ghose (1995)	4a
		1360 K	36.58	1.009	17.43	1.005	34.24	1.012		4b
	protopyroxene	1360 K	34.68	1.009			39.14	1.014		4c
	orthopyroxene	8.10 GPa	38.91	1.010	19.61	1.006	20.87	1.007	Hugh-Jones and Angel (1994)	5b
ferrosilite	HP-C2/c px	1.87 GPa	9.13	1.002			27.90	1.009	Hugh-Jones et al. (1994)	6
kosmochlor	HT-C2/c px	600 °C	18.03	1.004			29.19	1.009	Cameron et al. (1973)	1d
		1 atm	16.53	1.004			29.48	1.009	Origlieri et al. (2003)	7a
		9.28 GPa	11.46	1.003			28.06	1.009		7b
spodumene	HT-C2/c px	760 °C	19.02	1.005			43.90	1.015	Cameron et al. (1973)	1f
		0 GPa	18.08	1.005			44.62	1.015	Arlt and Angel (2000)	8a
		3.164 GPa	16.60	1.005			45.48	1.015		8b
	low clinopyroxene	3.342 GPa	21.73	1.006	17.66	1.005	36.50	1.012		8c
		8.835 GPa	20.42	1.005	13.74	1.003	33.91	1.011		8d
	protopyroxene	0 GPa	33.78	1.009			32.77	1.011	Yang et al. (1999)	9a
		2.03 GPa	32.03	1.008			31.19	1.010		9b
	HP-protopyroxene	2.50 GPa	27.23	1.007	14.11	1.004	26.79	1.009		9c
		9.98 GPa	27.80	1.007	13.26	1.004	22.27	1.007		9d
			σ_T	λ_T	σ_{M1}	λ_{M1}	σ_{M2}	λ_{M2}		
forsterite	olivine	25 °C	49.53	1.011	96.34	1.027	90.67	1.026	Takéuchi et al. (1984)	

Notes: Regular polyhedra have variance and elongation of zero and one, respectively. Numbers are assigned to the references for use in other tables.

TABLE 3. Structural parameters of various model *C2/c* pyroxenes

θ (°)	*r*	OE	*a*	*b*	*c*	β	T				O1	O2	O3	
							x	z	x	z	x	z	y	z
240	1		√(164/3)	6	2 √3	$\cos^{-1}$(-c/a)	5/16	19/48	1/8	5/24	3/8	7/24	−1/12	31/24
220	1		7.565	6.510	3.759	115.8	0.3100	0.3551	0.1301	0.1974	0.3699	0.3026	−0.0525	1.2101
200	1		7.608	6.823	3.939	113.4	0.3085	0.3204	0.1330	0.1856	0.3670	0.3144	−0.0255	1.1408
180	1		7.526	6.928	4	110.8	0.3080	0.2887	0.1340	0.1726	0.3660	0.3274	0	1.0774
160	1		7.326	6.823	3.939	107.7	0.3085	0.2576	0.1330	0.1585	0.3670	0.3415	0.0255	1.0152
140	1		7.023	6.510	3.759	104.1	0.3100	0.2248	0.1301	0.1427	0.3699	0.3573	0.0525	0.9497
120	1		2 √11	6	2 √3	$\cos^{-1}$(-c/3a)	5/16	3/16	1/8	1/8	3/8	3/8	1/12	7/8
166.4	1.318	1a	9.756	9.067	5.235	108.7	0.3082	0.2676	0.1335	0.1632	0.3665	0.3368	0.0172	1.0352
168.5	1.330	1b	9.876	9.170	5.294	109.0	0.3082	0.2709	0.1337	0.1647	0.3663	0.3353	0.0145	1.0419
166.4	1.319	2a	9.760	9.071	5.237	108.7	0.3082	0.2676	0.1335	0.1631	0.3664	0.3369	0.0172	1.0351
163.6	1.304	2b	9.607	8.939	5.161	108.3	0.3083	0.2632	0.1333	0.1611	0.3667	0.3389	0.0281	1.0264
138.3	1.366	6	9.552	8.844	5.106	103.8	0.3101	0.2219	0.1298	0.1413	0.3702	0.3587	0.3702	0.9438
172.0	1.294	1c	9.653	8.944	5.164	109.6	0.3081	0.2763	0.1338	0.1672	0.3662	0.3328	0.0100	1.0527
172.9	1.299	1d	9.697	8.980	5.184	109.7	0.3081	0.2776	0.1339	0.1677	0.3661	0.3323	0.0090	1.0552
172.8	1.292	7a	9.650	8.937	5.160	109.7	0.3081	0.2775	0.1339	0.1677	0.3661	0.3323	0.0091	1.0550
166.1	1.271	7b	9.401	8.738	5.045	108.7	0.3082	0.2672	0.1335	0.1630	0.3665	0.3370	0.0018	1.0343
189.5	1.263	1e	9.570	8.717	5.033	112.1	0.3081	0.3035	0.1337	0.1789	0.3662	0.3211	-0.0198	1.1070
186.6	1.267	1f	9.589	8.766	5.061	111.7	0.3081	0.2989	0.1339	0.1770	0.3661	0.3230	-0.0083	1.0979
189.9	1.263	8a	9.572	8.715	5.032	112.1	0.3081	0.3041	0.1337	0.1792	0.3663	0.3208	-0.0124	1.1082
189.5	1.254	8b	9.503	8.655	4.997	112.1	0.3081	0.3036	0.1338	0.1790	0.3662	0.3211	-0.0120	1.1072

Notes: M1 = [0 11/12 1/4], M2 = [0 1/4 1/4], $y_T = 1/12$, $y_{O1} = 1/12$, $y_{O2} = 1/4$, $x_{O3} = x_{O2}$. The column labeled OE contains the reference numbers (Tables 1 and 7) of the observed equivalents to the presented model structures. The structure with θ = 240 is hexagonal closest-packed and the structure with θ = 120 is cubic closest-packed (Thompson 1970; Papike et al. 1973; Thompson and Downs 2003).

TABLE 3—*continued*

θ (°)	*r*	OE	*a*	*b*	*c*	β	T				O1	O2	O3	
							x	z	x	z	*x*	*z*	*y*	*z*
180.8	1.287	10	9.695	8.919	5.149	110.9	0.3080	0.2900	0.1340	0.1732	0.3660	0.3268	-0.0010	1.0799
179.9	1.276	11	9.601	8.839	5.103	110.7	0.3080	0.2886	0.1340	0.1726	0.3660	0.3274	0.0001	1.0771
178.1	1.284	12	9.648	8.898	5.137	110.5	0.3080	0.2857	0.1340	0.1713	0.3660	0.3287	0.0024	1.0713
175.6	1.313	13	9.838	9.092	5.249	110.1	0.3080	0.2819	0.1339	0.1697	0.3661	0.3303	0.0055	1.0638
174.7	1.273	14	9.527	8.810	5.087	110.0	0.3080	0.2804	0.1339	0.1690	0.3661	0.3310	0.0067	1.0608
174.1	1.297	15	9.698	8.973	5.181	109.9	0.3081	0.2795	0.1339	0.1686	0.3661	0.3314	0.0074	1.0591
174.0	1.302	1g	9.737	9.009	5.201	109.9	0.3081	0.2794	0.1339	0.1685	0.3661	0.3315	0.0076	1.0587
173.9	1.310	16	9.791	9.060	5.231	109.9	0.3081	0.2793	0.1339	0.1685	0.3661	0.3315	0.0076	1.0586
173.7	1.328	17	9.929	9.189	5.305	109.8	0.3081	0.2790	0.1339	0.1683	0.3661	0.3317	0.0079	1.0579
173.0	1.300	18	9.712	8.992	5.192	109.7	0.3081	0.2779	0.1339	0.1679	0.3661	0.3321	0.0088	1.0558
172.7	1.291	19	9.640	8.928	5.155	109.7	0.3081	0.2773	0.1338	0.1676	0.3661	0.3324	0.0092	1.0246
171.0	1.338	20	9.967	9.241	5.335	109.4	0.3081	0.2748	0.1338	0.1665	0.3662	0.3335	0.0130	1.0496
165.2	1.316	21	9.724	9.043	5.221	108.5	0.3083	0.2657	0.1335	0.1623	0.3665	0.3377	0.0188	1.0314
165.1	1.325	22	9.785	9.100	5.254	108.5	0.3083	0.2655	0.1334	0.1622	0.3666	0.3378	0.0189	1.0310
164.4	1.332	23	9.828	9.142	5.278	108.4	0.3083	0.2644	0.1334	0.1617	0.3666	0.3383	0.0198	1.0289
163.8	1.348	24	9.940	9.248	5.339	108.3	0.3083	0.2635	0.1333	0.1613	0.3667	0.3387	0.0206	1.0270
161.3	1.329	25	9.755	9.083	5.244	107.9	0.3084	0.2596	0.1331	0.1594	0.3669	0.3406	0.0238	1.0193

TABLE 4. Structural parameters of various model low clinopyroxenes, space group $P2_1/c$

θA		240	180	202.8	197.1	203.2	206.4
θB		120	120	138.1	141.6	152.5	143.5
r		1	1	1.306	1.307	1.265	1.254
OE				3a	3b	8c	8d
a		4 √3	7.559	9.725	9.764	9.402	9.292
b		6	6.928	8.872	8.953	8.587	8.459
c		2 √3	4	5.122	5.169	4.958	4.884
β		$\cos^{-1}(-2c/3a)$	105.3	108.9	108.8	110.2	109.6
TA	*x*	1/16	0.0560	0.0580	0.0577	0.0585	0.0585
	z	3/8	0.2780	0.3148	0.3069	0.3179	0.3213
TB	*x*	9/16	0.5647	0.5608	0.5604	0.5590	0.5600
	z	5/24	0.1990	0.2321	0.2366	0.2533	0.2407
M1	*x*	1/4	0.2413	0.2471	0.2473	0.2495	0.2485
	z	1/6	0.2040	0.2060	0.2124	0.2172	0.2083
O1A	*x*	7/8	0.8880	−0.1159	−0.1154	−0.1171	−0.1170
	z	1/4	0.1940	0.2079	0.2013	0.2029	0.2091
O2A	*x*	1/8	0.1120	0.1159	0.1154	0.1171	0.1170
	z	1/4	0.3060	0.2921	0.2967	0.2971	0.2909
O3A	*y*	1/8	1/4	0.2791	0.2717	0.2796	0.2839
	z	3/4	0.5560	0.6295	0.6137	0.6359	0.6426
O1B	*x*	3/8	0.3707	0.3783	0.3791	0.3819	0.3801
	z	1/12	0.1020	0.1200	0.1261	0.1373	0.2091
O2B	*x*	5/8	0.6293	0.6217	0.6209	0.6181	0.6199
	z	5/12	0.3980	0.3800	0.3739	0.3627	0.3743
O3B	*y*	5/8	0.6293	0.6948	0.6209	0.7147	0.7024
	z	5/12	0.3980	0.4643	0.4732	0.5067	0.4815

Notes: $y_{TA} = y_{O1A} = 1/3$, $y_{TB} = 5/6$, $y_{M1} = 2/3$, M2 = [x_{M1} 0 z_{M1}], $y_{O2A} = 1/2$, $x_{O3A} = x_{O2A}$, $y_{O1B} = 5/6$, $y_{O2B} = 0$, $x_{O3B} = x_{O2B}$. The row labeled OE contains the reference numbers (Table 1) of the observed equivalents to the presented model structures. The structure with θA = 240 and θB = 120 is closest-packed and has stacking sequence ABABCACABCBC (Thompson and Downs 2003).

TABLE 5. Structural parameters of various model orthopyroxenes, space group *Pbca*

θA		180	180	158.9	163.0	158.7	158.5
θB		120	180	139.3	149.5	139.0	136.4
r		1	1	1.302	1.317	1.302	1.276
OE				4a	4b	5a	5b
a		14.580	14.074	18.363	18.535	18.363	18.027
b		6.928	6.928	8.867	9.024	8.864	8.683
c		4	4	5.119	5.210	5.118	5.013
TA	*x*	0.2780	0.2790	0.2789	0.2790	0.2789	0.2789
	z	0	13/12	1.0836	1.0872	1.0836	1.0804
TB	*x*	0.4677	0.4710	0.4697	0.4703	0.4696	0.4694
	z	5/6	3/4	0.8035	0.7894	0.8040	0.8077
M1	*x*	0.3707	3/8	0.3736	0.3743	0.3736	0.3733
	z	5/6	11/12	0.8631	0.8773	0.8627	0.8590
O1A	*x*	0.1940	0.1920	0.1921	0.1920	0.1921	0.1922
O2A	*x*	0.3060	0.3080	0.3079	0.3080	0.3079	0.3078
	z	0	13/12	1.0298	1.0440	1.0294	1.0256
O3A	*y*	1/4	1/4	0.2231	0.2284	0.2229	0.2226
	z	3/4	5/6	0.8605	0.8588	0.8608	0.8578
O1B	*x*	0.5647	0.5580	0.5607	0.5595	0.5607	0.5611
O2B	*x*	0.4353	0.4420	0.4393	0.4405	0.4393	0.4389
	z	2/3	3/4	0.6965	0.7106	0.6960	0.6923
O3B	*y*	1/6	1/4	0.1965	0.2106	0.1960	0.1923
	z	2/3	1/2	0.6071	0.5787	0.6079	0.6154

Notes: $y_{TA} = 1/3$, $y_{TB} = 1/3$, $y_{M1} = 2/3$, M2 = [x_{M1}, 1/2, $z_{M1} - 1/2$], $y_{O1A} = 1/3$, $z_{O1A} = z_{TA}$, $y_{O2A} = 1/2$, $x_{O3A} = x_{O2A}$, $y_{O1B} = 1/3$, $z_{O1B} = z_{TB}$, $y_{O2B} = 1/2$, $x_{O3B} = x_{O2B}$. The row labeled OE contains the reference numbers (Table 1) of the observed equivalents to the presented model structures.

TABLE 6. Structural parameters of various model protopyroxenes, space group *Pbcn*

θ	*r*	OE	*a*	*b*	*c*	T	O1	O2		O3	
						x	*x*	*x*	*z*	*y*	*z*
180	1		7.037	6.928	4	0.3080	0.1340	0.3660	1/12	0	1/3
168.4	1.321	4c	9.268	9.102	5.255	0.3082	0.1337	0.3663	0.1126	-0.0146	0.3187
166.2	1.312	9a	9.199	9.026	5.211	0.3082	0.1335	0.3665	0.1182	-0.0175	0.3159
165.9	1.306	9b	9.154	8.981	5.185	0.3082	0.1335	0.3665	0.1191	-0.0179	0.3155

Notes: M1 = [0 1/12 3/4], M2 = [0 1/4 1/4], $y_T = z_T = y_{O1} = z_{O1} = 1/12$, $y_{O2} = 1/4$, $x_{O3} = x_{O2}$. The column labeled OE contains the reference numbers (Table 1) of the observed equivalents to the presented model structures.

TABLE 7. Structural parameters of various model H*P*-protopyroxenes, space group $P2_1cn$

θA		120	154.0	147.8
θB		240	212.1	220.8
r		1	1.315	1.307
OE			9c	9d
a		8√6 /3	9.127	9.002
b		6	8.877	8.698
c		2 √3	5.125	5.022
TA	*x*	5/16	0.3088	0.3093
	z	0	0.0500	0.0416
O1A	*x*	1/8	0.1324	0.1315
O2A	*x*	3/8	0.3676	0.3685
	z	1/6	0.1167	0.1250
O3A	*y*	1/12	-0.0334	-0.0417
	z	1/6	0.2666	0.2499
TB	*x*	3/16	0.1920	0.1922
O1B	*x*	3/8	0.3709	0.3744
O2B	*x*	1/8	0.1324	0.1315
	z	0	0.0337	0.0178
O3B	*y*	5/12	0.4585	0.4464
	z	0	-0.0918	-0.0714
M1	*z*	2/3	0.7004	0.6845

Notes: $y_{TA} = y_{O1A} = 1/12$, $z_{O1A} = z_{TA}$, $y_{O2A} = 1/4$, $x_{O3A} = x_{O2A}$, $y_{TB} = 7/12$, $z_{TB} = z_{O2A}$, $y_{O1B} = 7/12$, $z_{O1B} = z_{TB}$, $y_{O2B} = 3/4$, $y_{M1} = 2/3$, $x_{O3B} = x_{O2B}$, $x_{M1} = 0$, $y_{M1} = 1/12$, M2 = [x_{M1} 1/4 z_{M1} – 1/2]. These models have regular tetrahedra. The row labeled OE contains the reference numbers (Table 1) of the observed equivalents to the presented model structures. The observed structures were reported with chain names reversed, i.e., $\theta A_{model} = \theta B_{observed}$. The structure with θA =120 and θB = 240 is closest-packed and has stacking sequence ABAC (Thompson and Downs 2003).

= 180°) model $C2/c$ pyroxene. Then the tetrahedral chains in alternating layers rotate in opposite directions from 180° to the ideal closest-packed $P2_1/c$ low clinopyroxene (θA = 240° and θB = 120°). From there, θB remains at 120° while TA rotates from θA = 240° to θA = 120°, resulting in the ideal CCP $C2/c$ pyroxene. This idealized phase transition sequence is based on a sequence of transitions observed in some lithium-bearing and other pyroxenes as temperature decreases or pressure increases (cf. Arlt and Armbruster 1997; Arlt et al. 1998; Arlt and Angel 2000b; Redhammer et al. 2001).

Figures 4 and 5 show that there is a volume maximum in a model pyroxene when a tetrahedral chain has θ = 180°. There must be some mechanism that compensates for this in actual pyroxenes during pressure-induced phase transitions where θ changes from less than 180° to greater than 180° or vice versa. During the pressure-induced transition from H*T*-$C2/c$ (3.164 GPa) to $P2_1/c$ (3.342 GPa) in spodumene (Arlt and Angel 2000b), the tetrahedral volume increases from 2.144 Å^3 to 2.149 Å^3 in the A-chain and to 2.159 Å^3 in the B-chain, while the M1 octahedral volume increases from 9.069 Å^3 to 9.126 Å^3. Just before the transition θ = 189.5°, and after the transition θA = 203.2° and θB = 152.5°. If θB rotates through 180°, then unit cell volume must increase unless there is a component of polyhedral compression followed by "reinflation". This seems unlikely; so perhaps the tetrahedra tilt so that all of the O3 atoms no longer

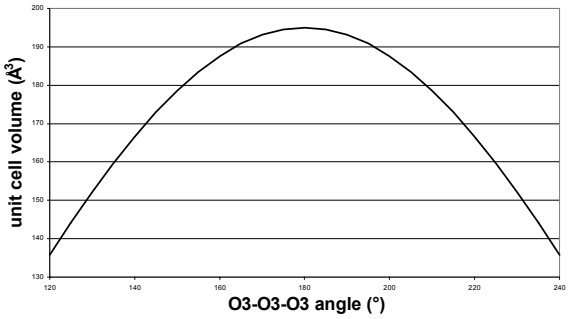

FIGURE 4. Unit cell volume vs. O3-O3-O3 angle for the model *C*2/*c* pyroxene with model O atom radius = 1 Å (tetrahedral volume is fixed). This figure shows that any pressure-induced transition that changes a tetrahedral chain orientation from O-rotated to S-rotated or vice versa is fighting a volume increase.

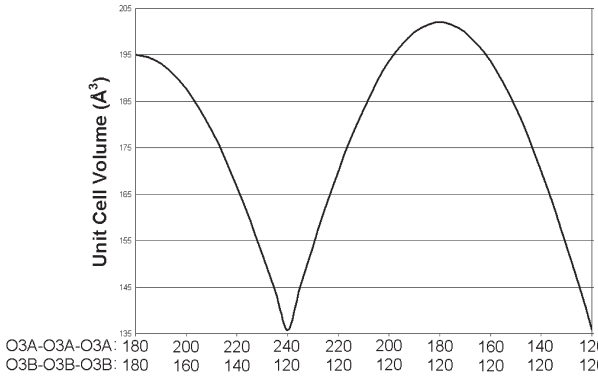

FIGURE 5. Unit cell volume vs. O3A-O3A-O3A and O3B-O3B-O3B for an idealized phase transition sequence: H*T*-*C*2/*c* pyroxene → low clinopyroxene → H*P*-*C*2/*c* pyroxene. This figure again shows that any pressure-induced transition that changes a tetrahedral chain orientation from O-rotated to S-rotated or vice versa is fighting a volume increase.

have the same *x*-coordinate, temporarily destroying the **c**-glide. This would allow the B-chain to change its orientation without rotating through a volume maximum or forcing some sort of temporary polyhedral volume decrease.

Examination of the model equivalents to the observed H*T*-*C*2/*c* spodumene structure at 3.164 GPa and the observed $P2_1/c$ structure at 3.342 GPa (Arlt and Angel 2000b) shows that the changes in θA and θB across the transition produce a larger model cell volume decrease than the observed cell volume decrease. Thus, there is a component of isotropic expansion necessary in the model transition, as reflected in the model O atom radius increase across the transition from the model H*T*-*C*2/*c* spodumene structure to the model $P2_1/c$ structure (pyroxene 8b in Table 3 and 8c in Table 4). This is consistent with the polyhedral volume increases across the observed transition.

Interatomic distances

Various hypotheses have been put forward to explain the variation of θ in *C*2/*c* pyroxenes. Thompson (1970) pointed out that T shares an edge with M2 when θ = 240° but not when θ = 120°, and suggested that nature will therefore prefer θ closer to 120° (Fig. 6). Papike et al. (1973) correlated θ with average cation size. Thompson and Downs (2003) presented evidence that the M2-T repulsion across the shared edge is more important in determining θ than cation size.

It is useful to define some crystallographic parameters in order to examine the effect of M2-T repulsion on θ. Some model and observed data are listed in Table 8 for the M2-T and M1-T distances that are illustrated in Figure 6. The relevant M1 and M2 octahedra share O2 with the tetrahedron. Figure 6 illustrates these distances for the closest-packed ideal *C*2/*c* pyroxenes, quantitatively discussed in the introduction. Also, each tetrahedron shares O1 with two additional M1 octahedra (Fig. 1). The average of these two M1-T distances is called <M1'-T> in Table 8 (these distances are always equal in the model, but differ slightly in real pyroxenes). Figure 7 illustrates how these three distances vary in the model pyroxene as θ varies between 120° and 240°. Figure 7 also contains data points for 20 observed *C*2/*c* pyroxenes at room conditions plus ferrosilite (Hugh-Jones et al. 1994) at 1.87 GPa (Table 8). The model O atom radius, *r*, was arbitrarily set to 4/3 in order to put the M2-T curve through the data points for the observed pyroxenes, facilitating comparison.

The variation of the model M2-T distance with θ is illustrated in Figure 7. This distance is essentially constant over the domain 120° ≤ θ ≤ 150°. As θ increases from 150° to 240°, *R*(M2-T) decreases at an ever-increasing rate. This is because model unit cell volume reaches a maximum when θ = 180°, so that the volume increase as θ goes from 120° to 180° initially more than compensates for the decrease in M2-T brought about by tetrahedral rotation. After 180°, volume decreases, adding its own component of shortening to that brought about tetrahedral rotation alone.

The variation of the model M1-T distance with θ is also the result of a combination of tetrahedral rotation and cell volume change. However, T is rotating away from M1 as it rotates toward M2, so $R(\text{M1-T})_{240°} > R(\text{M1-T})_{120°}$.

With the exception of M1-T and M2-T, all model nearest neighbor cation-anion, cation-cation, and anion-anion distances vary symmetrically about 180° as a function of θ. For example, the plot in Figure 7 of the <M1'-T> distance as a function of θ is symmetric about 180° and maximal at 180°. This is a consequence of the volume change and is typical of the variation of most model interatomic distances.

There must be other important crystallographic parameters in-

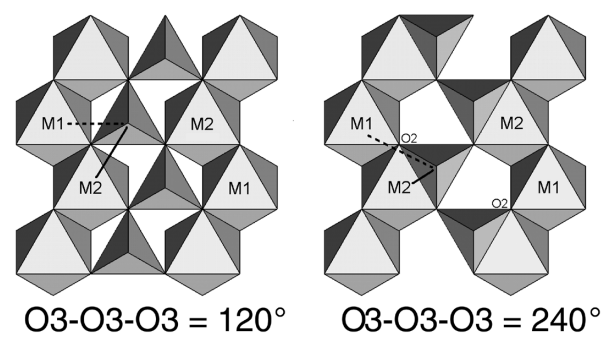

FIGURE 6. Portions of two model *C*2/*c* pyroxenes showing the very short M2-T distance when O3-O3-O3 = 240°.

TABLE 8. Selected crystallographic parameters for *C*2/*c* pyroxenes at ambient conditions plus ferrosilite at 1.87 GPa

M2M1	θ (°)	Model *r*	M2-T	Model M2-T	M1-T	Model M1-T	<M1'-T>	Model M1'-T	*c*/*b*	Reference	Ref no.
LiAl	189.8	1.263	2.862	2.723	3.277	3.50	3.145	3.21	0.622	Arlt and Angel (2000)	8a
LiFe	180.8	1.287	2.936	2.854	3.340	3.62	3.244	3.33	0.611	Redhammer et al. (2001)	10
LiGa	179.9	1.276	2.915	2.835	3.307	3.52	3.209	3.25	0.615	Sato et al. (1994)	11
LiV	178.1	1.284	2.915	2.869	3.361	3.54	3.238	3.27	0.618	Satto et al. (1997)	12
LiSc	175.6	1.313	2.961	2.951	3.425	3.61	3.326	3.34	0.597	Hawthorne and Grundy (1977)	13
NaAl	174.7	1.273	2.985	2.867	3.308	3.49	3.153	3.24	0.610	Clark et al. (1969)	14
NaMn	174.1	1.297	3.050	2.925	3.361	3.55	3.266	3.30	0.621	Ohashi et al. (1987)	15
NaFe	174.0	1.302	3.028	2.938	3.378	3.57	3.239	3.31	0.602	Cameron et al. (1973)	1g
NaTi	173.9	1.310	3.025	2.955	3.424	3.59	3.267	3.33	0.597	Ohashi et al. (1982)	16
NaSc	173.7	1.328	3.038	2.998	3.465	3.64	3.317	3.38	0.591	Ohashi et al. (1994A)	17
NaV	173.0	1.300	3.013	2.934	3.394	3.56	3.241	3.31	0.606	Ohashi et al. (1994B)	18
NaCr	172.8	1.292	2.995	2.924	3.379	3.54	3.211	3.29	0.605	Origlieri et al. (2003)	7a
NaGa	172.7	1.291	3.003	2.922	3.345	3.53	3.205	3.28	0.606	Ohashi et al. (1995)	19
NaIn	171.0	1.338	3.041	3.038	3.486	3.65	3.344	3.40	0.588	Ohashi et al. (1990)	20
CaMg	166.5	1.319	3.095	3.022	3.480	3.57	3.236	3.34	0.589	Levien and Prewitt (1981)	2a
CaNi	165.2	1.316	3.097	3.024	3.474	3.56	3.234	3.33	0.588	Ghose et al. (1987)	21
CaCo	165.1	1.325	3.111	3.044	3.492	3.58	3.267	3.35	0.586	Ghose et al. (1987)	22
CaFe	164.4	1.332	3.126	3.065	3.511	3.60	3.295	3.37	0.581	Zhang et al. (1997)	23
CaMn	163.8	1.348	3.126	3.106	3.561	3.64	3.327	3.41	0.578	Freed and Peacor (1967)	24
ZnZn	161.3	1.329	3.063	3.073	3.437	3.57	3.316	3.35	0.578	Morimoto et al. (1975)	25
FeFe	138.3	1.366	3.156	3.224	3.425	3.45	3.295	3.34	0.557	Hugh-Jones et al. (1994)	6

Notes: Model data is included for comparison. Interatomic distances are in angstroms. Model $c/b = 1/\sqrt{3} = 0.577$. M1-T and M2-T distances are for cations sharing coordination with O2. <M1'-T> is the average the two M1-T distances for the cations sharing O1 (these distances can vary slightly in observed pyroxenes but are always equal in the models). Model equivalents for these pyroxenes are in Table 2.

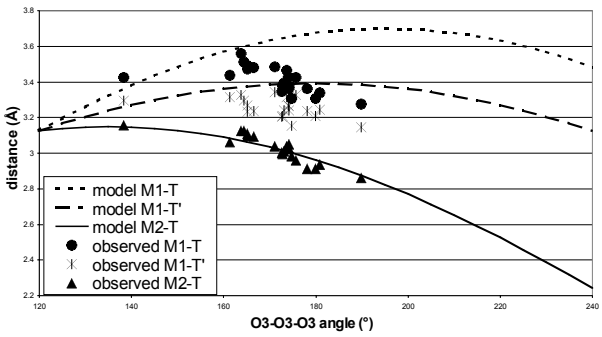

FIGURE 7. Comparison of some model M-T distances as a function of O3-O3-O3 angle with 20 ambient condition and one high-pressure *C*2/*c* pyroxenes. Model O atom radius = 4/3 Å. This illustrates the very short M2-T distance at O3-O3-O3 = 240° and the elongation of M2-T in the observed pyroxenes relative to the other observed M-T distances in comparison to the model proportions.

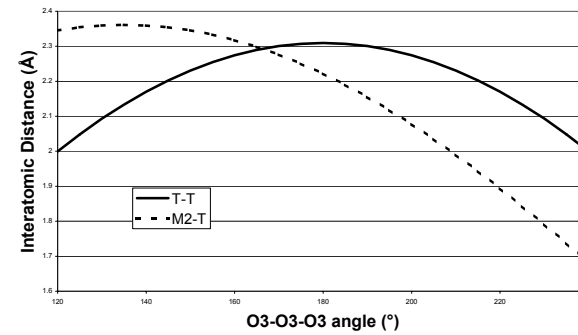

FIGURE 8. M2-T and T-T distances for the model *C*2/*c* pyroxene as a function of O3-O3-O3 angle when the model O atom radius = 1 Å. These competing repulsions provide a general explanation for the topology of ambient condition *C*2/*c* pyroxenes. If M2 is univalent, then T-T repulsion dominates and θ ~180°. If M2 is divalent, then the M2-T repulsion is strong enough to drive θ to ~165° or less.

fluencing θ, or θ would approximate 120° in observed pyroxenes, since this maximizes *R*(M2-T). Thompson and Downs (2003) hypothesized that T-T distances in the tetrahedral chains favor θ = 180°. Figure 8 illustrates *R*(M2-T) and *R*(T-T) as a function of θ when *r* = 1. These competing repulsions provide a general explanation for the geometry of the tetrahedral chains in ambient condition *C*2/*c* pyroxenes. If M2 is univalent, then T-T repulsion dominates and θ ~180°. If M2 is divalent, then the M2-T repulsion is strong enough to drive θ to ~165° or less.

In addition to suggesting that M2-T repulsion is important in determining θ, Figure 7 suggests that this repulsion is important in distorting a given observed pyroxene from its model configuration. The figure shows that the M2-T distance in the observed pyroxenes is elongated relative to the observed M1-T and <M1'-T> distances in comparison to the model proportions, and that this elongation systematically increases with increasing θ. This may explain some of the bonding around M2 in the observed zinc pyroxene and various Li-bearing pyroxenes as determined by electron density analysis (Downs 2003). In the absence of other forces, M2 would move to a position as nearly equidistant from all of the surrounding O atoms as possible, but the M2-T repulsion pushes M2 away from a central position, so much so that M2 may not be bonded to O3.

Relative elongation of the **c**-axis keeps *R*(M2-T) as long as possible. In all model pyroxenes, $c/b = 1/\sqrt{3} = 0.577$. In all of the observed ambient *C*2/*c* pyroxenes, this ratio is larger.

Bonding transitions in clinopyroxenes

The purpose of this section is to explain the inconsistency between packing and bonding topology in *C*2/*c* pyroxenes by analyzing model M2-O3 distances.

Figure 9 illustrates a nomenclature (after Downs 2003) that we will use to discuss the bonding around M2. The O3s that can be bonded to M2 are labeled $O3_1$, $O3_2$, $O3_3$, and $O3_4$. These labels

are relative to a given M2; i.e., $O3_4$ relative to the illustrated M2 is $O3_3$ relative to the adjacent M2 that is not shown. The labeling of the O atoms around a given M2 can be done by viewing down **a*** and locating the "arrowhead" formed by the two octahedral faces sharing an edge (northwest of M2 in Fig. 9). Burnham et al. (1967) presented an alternative nomenclature, giving every atom in the unit cell its own name (in Fig. 9, $O3_1$ = O3C2, $O3_2$ = O3C1, $O3_3$ = O3D1, and $O3_4$ = O3D2). We use the nomenclature of Downs (2003) because it provides a single description that applies to every M2 in the structure.

Thompson and Downs (2003), building on terminology from Yang and Prewitt (2000), defined three categories of *C*2/*c* pyroxenes using bonding topology and phase transition pathway criteria. In the *C*2/*c* structures, the M2 atom occurs on a twofold rotation axis. This position constrains its coordination numbers to four, six, or eight, because M2 is bonded to two O1 atoms, two O2 atoms and either zero, two, or four O3 atoms. $O3_2$ and $O3_3$ are always the same distance from M2, and $O3_1$ and $O3_4$ are also equidistant from M2. Thus, there are two different possible six-coordinated bonding topologies. H*T*-*C*2/*c* pyroxene has M2 bonded to $O3_2$ and $O3_3$. This bonding topology occurs when $R(M2\text{-}O3_{2,3})$ is short and $R(M2\text{-}O3_{1,4})$ is long. H*P*-*C*2/*c* pyroxene has M2 bonded to $O3_1$ and $O3_4$. This bonding topology occurs when $R(M2\text{-}O3_{1,4})$ is short and $R(M2\text{-}O3_{2,3})$ is long. Eight-coordinated M2-*C*2/*c* pyroxene has M2 bonded to all four O3 atoms. This bonding topology occurs when both $R(M2\text{-}O3_{2,3})$ and $R(M2\text{-}O3_{1,4})$ are short enough. Observed clinopyroxenes with four-coordinated M2 (no M2-O3 bonds) go through a pressure and/or temperature induced transition sequence from *C*2/*c* to $P2_1/c$ to *C*2/*c*. We define the high-temperature, low-pressure *C*2/*c* phase as H*T*-*C*2/*c* pyroxene, and the low-temperature, high-pressure *C*2/*c* phase as H*P*-*C*2/*c* pyroxene.

Figure 10 shows the variations of model M2-O3 distances with θ. For a given O atom radius, *r*, M2-O3 distances depend only on θ: $R(M2\text{-}O3_{2,3})$ is short and $R(M2\text{-}O3_{1,4})$ is long when θ > ~167°, $R(M2\text{-}O3_{1,4})$ is short and $R(M2\text{-}O3_{2,3})$ is long when θ < ~140°, and both $R(M2\text{-}O3_{2,3})$ and $R(M2\text{-}O3_{1,4})$ are relatively short when ~140° < θ < ~167°. The correspondence between bonding topology and θ suggested by the model is observed in real pyroxenes, i.e., H*T*-*C*2/*c* pyroxene occurs when θ > ~167°, H*P*-*C*2/*c* pyroxene occurs when θ < ~140°, and eight-coordinated M2-*C*2/*c* pyroxene occurs when ~140° < θ < ~167°. θ domains for observed pyroxene bonding topologies are indicated on Figure 10.

At the point where all four bond lengths are equal, θ = 158.2°, the model M2 must be either four- or eight-coordinated. Bindi et al. (2002) reported a potassium-rich eight-coordinated M2-*C*2/*c* pyroxene with nearly equal M2-O3 distances, 2.789 Å and 2.796 Å, that has θ = 158.7°, consistent with the model. Published and unpublished pressure data sets suggest that most eight-coordinated M2-*C*2/*c* pyroxenes have all four M2-O3 bond lengths equal at some point in the domain 156° ≤ θ ≤ 161°.

Packing, however, can be considered to change at θ = 180°. The structure is closer to HCP than CCP over the domain 180° < θ ≤ 240°, and closer to CCP than HCP over the domain 120° ≤ θ < 180°. This is explored in detail in the packing section below. The θ domains for the two packing schemes are indicated on Figure 10. To sum up, both packing and bonding topology

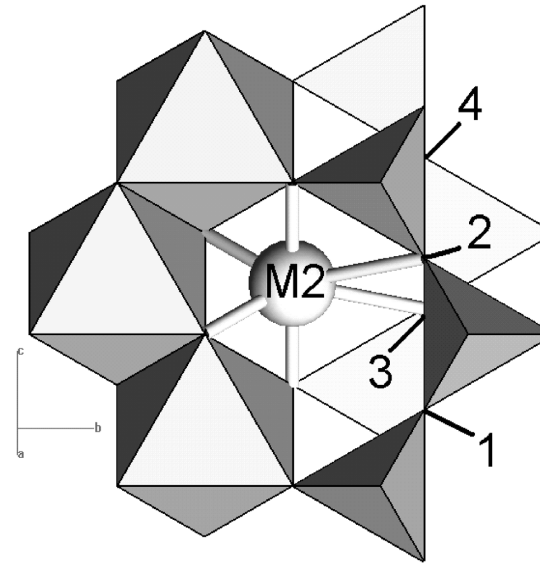

FIGURE 9. Portion of a model *C*2/*c* pyroxene with nomenclature (after Downs 2003) used to discuss the bonding around M2. The O3 atoms that can be bonded to M2 are labeled $O3_1$, $O3_2$, $O3_3$, and $O3_4$. These labels are relative to a given M2; i.e., $O3_4$ relative to the illustrated M2 is $O3_3$ relative to the adjacent M2 that is not shown. The labeling of the O atoms around a given M2 can be done by viewing down **a*** and locating the "arrowhead" formed by the two octahedral faces sharing an edge (northwest of M2 in Fig. 9). Burnham et al. (1967) presented an alternative nomenclature, giving every atom in the unit cell its own name (in Fig. 9, $O3_1$ = O3C2, $O3_2$ = O3C1, $O3_3$ = O3D1, and $O3_4$ = O3D2). We use the nomenclature of Downs (2003) because it provides a single description that applies to every M2 in the structure.

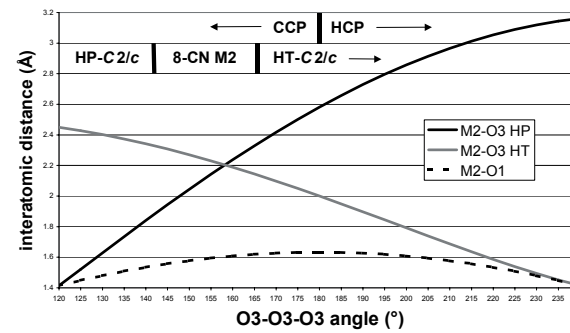

FIGURE 10. M2-O3 interatomic distances for the model *C*2/*c* pyroxene as a function of O3-O3-O3 angle when the model O atom radius = 1 Å. Each solid line represents two equal M2-O3 distances because a twofold runs through M2. The line labeled H*P* represents the distances for the two O atoms bonded to M2 in H*P*-*C*2/*c* pyroxene ($O3_1$ and $O3_4$ in Fig. 9) – this bonding topology occurs in observed pyroxenes when the O3-O3-O3 angle is ~140° or less; the line labeled H*T* represents the distances for the two O atoms bonded to M2 in H*T*-*C*2/*c* pyroxene ($O3_2$ and $O3_3$ in Fig. 9) – this bonding topology occurs when the O3-O3-O3 angle is greater than ~167°. When both pairs of O3 atoms are relatively close to M2 (140° < O3-O3-O3 < 167°), then M2 is bonded to both pairs (all four O3 atoms). O3-O3-O3 domains for the different bonding topologies and for the packing arrangements of *C*2/*c* pyroxenes are demarcated. Packing and bonding topology both depend on O3-O3-O3 angle, but have different O3-O3-O3 angle domains.

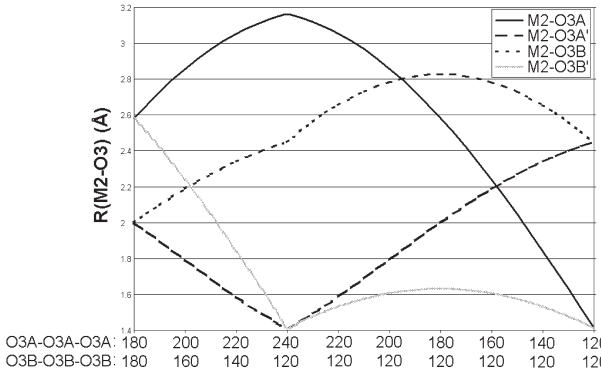

FIGURE 11. M2-O3 distances for the idealized phase transition sequence: H*T*-*C*2/*c* pyroxene → low clinopyroxene → H*P*-*C*2/*c* pyroxene. When two intermediate distances are equal, model low clinopyroxene cannot have six-coordinated M2.

depend on θ, but their θ domains do not correspond.

Figure 11 illustrates the model M2-O3 interatomic distances in low clinopyroxene as a function of θ when $r = 1$ for the model transition pathway discussed in the unit cell volume section. M2 in low clinopyroxene is on a general position so that all four possible M2-O3 interatomic distances are nonequivalent. Electron density analysis (Downs 2003) of spodumene at 3.342 GPa (Arlt and Angel 2000a) shows that M2 is five-coordinated. This is consistent with the model equivalent, which has the nearest M2-O3A, O3B, O3B, O3A distances at 2.225, 2.671, 2.872, and 3.625 Å, respectively.

Variations in cell angle β

Various authors have suggested explanations for observed variation of β with temperature and pressure in the *C*2/*c* pyroxenes (cf. Tribaudino 1996; Downs 2003). The model shows that tetrahedral rotation alone is sufficient to change β, as illustrated in Figure 12. Figure 12 compares the model relationship with observed data for diopside at *P* (Levien and Prewitt 1981) and *T* (Cameron et al. 1973), hedenbergite at *P* (Zhang et al. 1997) and *T* (Cameron et al. 1973), and kosmochlor at *P* (Origlieri et al. 2003) and *T* (Cameron et al. 1973). The pressure data appears to correlate well with the model, but the temperature data varies from a nice match with hedenbergite to an opposite trend with kosmochlor.

Orthorhombic pyroxenes

Analysis of model orthopyroxene gives insight into the stability of orthopyroxene at pressure and temperature. Figure 13 is a plot of bond angle variance for the M1 octahedron against θA. This curve is independent of θB. When θA = 240°, the structure is so distorted that model M1 can only be five- or seven-coordinated. Orthopyroxene cannot have regular TA and M1 unless θA = 180°. If θA ≠ 180°, then one of the polyhedra must distort, and the farther from 180°, the more distorted. θA = 180° is a maximum volume arrangement, so orthopyroxene can only approach a model with regular polyhedra at temperature and has a built-in structural pressure instability. The same is true of protopyroxene.

Observed $P2_1cn$ high-*P* protopyroxene has two nonequivalent tetrahedral chains in the same tetrahedral layer and maintaining small values of polyhedral distortion for these tetrahedra may be important in determining the topology of this polymorph. Model $P2_1ca$ and $P2_1cn$ orthorhombic pyroxenes have tetrahedral layers with two nonequivalent tetrahedral chains (one pointing up **a***, one pointing down), and these chains must be rotated the same amount away from 180° for all polyhedra to be regular. Observed $P2_1cn$ pyroxene at 2.50 GPa (Yang et al. 1999) has TA and TB rotated in opposite directions away from 180°, by 32.1° and 26.0°, respectively. Yet, this θB results in a very short *R*(M2-TB) of 2.745 Å. Compare this with *R*(M2-TA) of 3.071 Å. This suggests that there is an energetic benefit to keeping the amount of rotation away from 180° in TA and TB nearly equal, and that this benefit more than compensates for the resulting short, high-energy M2-TB interatomic distance. This arrangement allows T and M1 to be nearly regular, suggesting that maintaining regular polyhedra may be important in determining the topology of observed structures.

The names of the tetrahedral chains in our model $P2_1cn$ pyroxene are reversed from those used by Yang, et al. (1999), i.e., $\theta A_{model} = \theta B_{observed}$, because TA in all other described pyroxenes

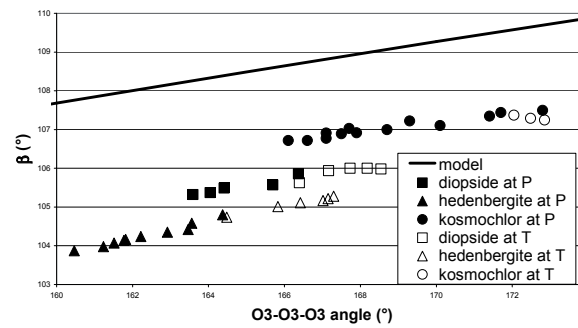

FIGURE 12. Comparison of the model relationship between β and O3-O3-O3 angle with the observed for diopside at *P* (Levien and Prewitt 1981) and *T* (Cameron et al. 1973), hedenbergite at *P* (Zhang et al. 1997) and *T* (Cameron et al. 1973), and kosmochlor at *P* (Origlieri et al. 2003) and *T* (Cameron et al. 1973). The pressure data appears to correlate well with the model, but the temperature data varies from a nice match with hedenbergite to an opposite trend with kosmochlor.

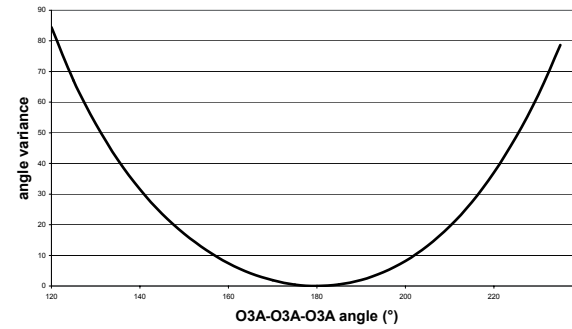

FIGURE 13. Bond angle variance for the model orthopyroxene as a function of O3A-O3A-O3A angle. This curve is independent of θB. θA = 180° is a maximum volume arrangement, so orthopyroxene can only approach a model with regular polyhedra at temperature and has a built-in structural pressure instability. The same is true of protopyroxene.

we have found in the literature has the shorter M2-T distance, the straighter chain, and the smaller volume. Yang et al.'s (1999) choice keeps TB O-rotated, like low clinopyroxene, but this is a result of the alternating tilts between adjacent planes of octahedra. The θ = 240° in Figure 6 becomes 120° if the octahedral chain at the apices of the tetrahedra (not shown) has tilt reversed relative to the illustrated octahedra.

In structures with nonequivalent tetrahedral chains, our model suggests that the tetrahedra in the straighter chains should have the smaller volumes. This is observed in orthopyroxene, low clinopyroxene, and $P2_1cn$ high-pressure protopyroxene.

Compressional anisotropy

A comparison of strain ellipsoids for various observed pyroxenes and their equivalent models shows that a combination of tetrahedral rotation and isotropic compression approximates the compressional anisotropy observed in pyroxenes, except across phase boundaries (Table 9). However, the models did not consistently approximate strain ellipsoids for thermal expansion.

Axial ratios for strain ellipsoids of model orthorhombic pyroxenes have the form $x : y : y$ because the ratio of b/c is fixed ($\sqrt{3}$) and ellipsoidal axes are constrained to be parallel to crystallographic axes. High-pressure diffraction experiments on orthoenstatite (Hugh-Jones and Angel 1994) and synthetic protopyroxene (Yang et al. 1999) show that **b** is much more compressible than **c**, in contrast to the model.

Packing

Figure 14 illustrates the relationship between distortion from ideal closest-packing and θ for the model $C2/c$ pyroxenes. The isotropic distortion parameter, U_{CP}, (Thompson and Downs 2001) is used to quantify the distortion in the anion skeletons of the models. U_{CP} is the average mean square displacement of the anions in an observed structure from its best-fit closest-packed equivalent. Thus, a perfectly closest-packed structure has $U_{CP} = 0$. Larger values of U_{CP} indicate more structural distortion from closest-packing. A model O atom radius of 4/3 Å was used in the calculations. This is the O atom radius for the model hedenbergite at ambient conditions. Figure 14 illustrates the model distortion from CCP over the domain 120° ≤ θ ≤ 180° and the distortion from HCP over the domain 180° ≤ θ ≤ 240°. The model is ideal CCP at θ = 120° and ideal HCP at θ = 240°. Model distortion increases as θ approaches 180° from either direction in nearly identical quadratic or cubic fashion ($R^2_{CCP} = 0.9997$ and 1, respectively). Thus, it is reasonable to describe $C2/c$ pyroxenes with θ < 180° as distorted CCP and $C2/c$ pyroxenes with > 180° as distorted HCP.

Figure 14 compares the distortion in the model to the distortion in some observed pyroxenes at pressure and temperature.

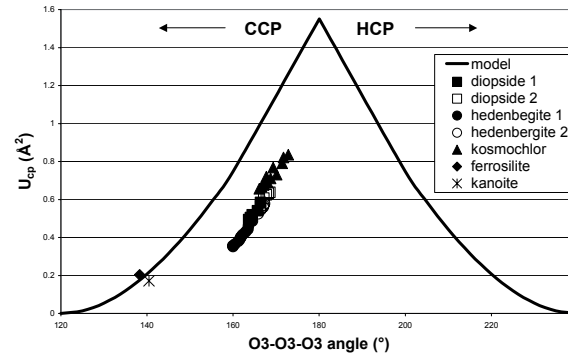

FIGURE 14. Distortion from closest-packing, U_{CP}, for the anion skeleton of the model $C2/c$ pyroxene as a function of the O3-O3-O3 angle. U_{CP} is the average mean square displacement of the anions in an observed structure from its best-fit closest-packed equivalent. Thus, a perfectly closest-packed structure has $U_{CP} = 0$. Larger values of U_{CP} indicate more structural distortion from closest-packing. The model is ideal CCP at O3-O3-O3 = 120°, reaches a maximum distortion at O3-O3-O3 = 180°, and moves to ideal HCP at O3-O3-O3 = 240°. This curve shows that it is reasonable to consider the packing of $C2/c$ pyroxenes with O3-O3-O3 < 180° as distorted CCP and the packing of $C2/c$ pyroxenes with O3-O3-O3 > 180° as distorted HCP. The lesser distortion from closest-packing in observed pyroxenes compared to their model equivalents is consistent with distortion from model configuration to minimize anion-anion repulsion. References are: diopside 1 = Levien and Prewitt (1981), diopside 2 = Cameron et al. (1973), hedenbergite 1 = Zhang et al. (1997), hedenbergite 2 = Cameron et al. (1973), kosmochlor = Origlieri et al. (2003), ferrosilite = Hugh-Jones et al. (1994), kanoite = Arlt and Armbruster (1997).

TABLE 9. Comparison of strain ellipsoids for various observed and model pyroxenes

Pyroxene	Phase	Δ*P* (GPa)	Axial ratios	Model	Orientation (°)	Model	Ref no.
diopside	8-CN M2 *C2/c*	0–5.3	1 : 2.3 : 2.3	1 : 1.5 : 1.8	53	58	2a,b
kosmochlor	H*T*-*C2/c*	0–9.28	1 : 1.8 : 2.1	1 : 1.9 : 2.6	50	60	7a,b
spodumene	H*T*-*C2/c*	0–3.164	1 : 1.6 : 1.7	1 : 1.1 : 1.1	70	71	8a,b
	low clinopyroxene	3.342–8.835	1 : 1.3 : 1.9	1 : 2.5 : 2.9	36	46	8c,d
enstatite	orthopyroxene	0–8.1	1 : 1.6 : 1.2	1 : 1.1 : 1.1	0	0	5a,b
	protopyroxene	0–2.03	1 : 1.7 : 1.0	1 : 1.0 : 1.0	0	0	9a,b
	hi-*P* protopyroxene	2.50–9.98	1 : 1.3 : 1.7	1 : 1.5 : 1.5	0	0	9c,d
		Δ*T* (°C)					
diopside	8-CN M2 *C2/c*	24–1000	1 : 6.8 : 3.2	1 : 1.4 : 1.6	59	60	1a,b
kosmochlor	H*T*-*C2/c*	24–600	1 : 1.2 : 0.4	1 : 1.5 : 1.9	39	64	1c,d
spodumene	H*T*-*C2/c*	24–760	1 : 1.2 : 0.2	1 : 0.6 : 0.1	60	70	1e,f
enstatite	low clinopyroxene	20–700	1 : 3.2 : 3.9	1 : 1.0 : 0.4	54	94	3a,b
	orthopyroxene	23–1087	1 : 1.5 : 1.5	1 : 1.9 : 1.9	0	0	4a,b
	Pressure-induced transitions	Δ*P* (GPa)					
spodumene	H*T*-*C2/c* – low clinopyroxene	3.164–3.342	1 : -2.9 : -11.0	1 : -0.5 : -1.4	42	58	8b,c
	proto–hi-*P* protopyroxene	2.03–2.50	1 : -0.9 : 2.2	1 : 3.9 : 3.9	0	0	9b,c

Notes: Ellipsoid axes, ε_1, ε_2, and ε_3, are oriented as follows. ε_2 is parallel to **b**; ε_1 and ε_3 are in the **ac**-plane and perpendicular to each other. The orientation given in the table is $\angle(\mathbf{a} \wedge \varepsilon_1)$, where ε_1 lies within acute $\angle(\mathbf{a} \wedge \mathbf{c})$, dividing β. In the orthorhombic pyroxenes, ε_1 is parallel to **a**. Axial ratios are $\varepsilon_1 : \varepsilon_2 : \varepsilon_3$. Ellipsoids were calculated using the STRAIN software by Ohashi (Hazen and Finger 1982).

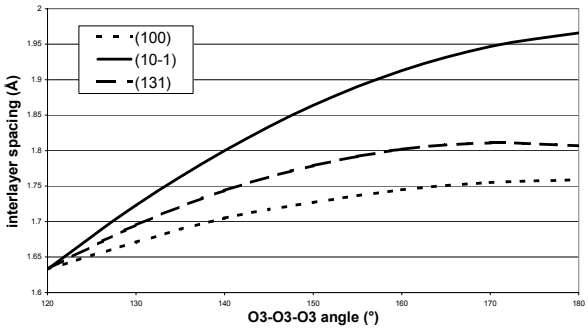

FIGURE 15. Interlayer spacing for the four stacking directions in CCP-based model *C*2/*c* pyroxene as a function of the O3-O3-O3 angle. Stacking directions are perpendicular to (100), $(10\bar{1})$, (131), and $(1\bar{3}1)$. (131) and $(1\bar{3}1)$ always have the same interlayer spacing.

Most of the observed structures are much less distorted than their model equivalents. This difference is slightly exaggerated in this figure if the model equivalent has a smaller model O atom radius than 4/3 Å (e.g., model O atom radius for kosmochlor is 1.292 Å). The small distortion from closest-packing of the observed pyroxenes in comparison with their model equivalents is consistent with the distortion of the observed structures from their model configurations to minimize anion-anion repulsion.

Figure 15 is a plot of the interlayer spacings vs. θ in the four stacking directions in CCP-based clinopyroxene. The four stacking directions are perpendicular to (100), (101bar), and (131) ≡ $(1\bar{3}1)$ (Thompson and Downs 2003). Origlieri et al. (2003) suggested that observed differences among these interlayer spacings are important to the compressional behavior of some clinopyroxenes. Figure 15 shows that model geometry creates differences.

ACKNOWLEDGEMENTS

We thank M. Tribaudino and F.E. Brenker for their time and valuable suggestions. We also thank the National Science Foundation for funding our study, Compression Mechanisms of Upper Mantle Minerals, through grant no. EAR-9903104.

REFERENCES CITED

Arlt, T. and Angel, R.J. (2000a) Pressure buffering in a diamond anvil cell. Mineralogical Magazine, 64, 241–245.

——— (2000b) Displacive phase transitions in C-centered clinopyroxenes: spodumene, $LiScSi_2O_6$ and $ZnSi_2O_6$. Physics and Chemistry of Minerals, 27, 719–731.

Arlt, T. and Armbruster, T. (1997) The temperature-dependent $P2_1/c$–C2/c phase transition in the clinopyroxene kanoite $MnMg(Si_2O_6)$: a single-crystal X-ray and optical study. European Journal of Mineralogy, 9, 953–964.

Arlt, T., Angel, R.J., Miletich, R., Armbruster, T., and Peters, T. (1998) High-pressure $P2_1/c$-*C*2/*c* phase transitions in clinopyroxenes: influence of cation size and electronic structure. American Mineralogist, 83, 1176–1181.

Bindi, L., Safonov, O.G., Litvin, Y.A., Perchuk, L.L., and Menchetti, S. (2002) Ultrahigh potassium content in the clinopyroxene structure: an X-ray single-crystal study. European Journal of Mineralogy, 14, 929–934.

Burnham, C.W., Clark, J.R., Papike, J.J., and Prewitt, C.T. (1967) A proposed crystallographic nomenclature for clinopyroxene structures. Zeitschrift für Kristallographie, 125, 109–119.

Cameron, M. and Papike, J.J. (1981) Structural and chemical variations in pyroxenes. American Mineralogist, 66, 1–50.

Cameron, M., Sueno, S., Prewitt, C.T., and Papike, J.J. (1973) High-temperature crystal chemistry of acmite, diopside, hedenbergite, jadeite, spodumene, and ureyite. American Mineralogist, 58, 594–618.

Chisholm, J.E. (1981) Pyribole structure types. Mineralogical Magazine, 44, 205–216.

——— (1982) Lowering of symmetry in pyribole structures. Mineralogical Magazine, 45, 25–34.

Clark, J.R., Appleman, D.E., and Papike, J.J. (1969) Crystal-chemical characterization of clinopyroxenes based on eight new structure refinements. Mineralogical Society of America Special Paper 2, 31–50.

Deer, W.A., Howie, R.A., and Zussman, J. (1978) Rock-Forming Minerals. Volume 2A, Second Edition, Single Chain Silicates. John Wiley, New York.

Downs, R.T. (2003) Topology of the pyroxenes as a function of temperature, pressure and composition determined from the procrystal electron density. American Mineralogist, 88, 556–566.

Freed, R.L. and Peacor, D.R. (1967) Refinement of the crystal structure of johannsenite. American Mineralogist, 52, 709–720.

Ghose, S., Wan, C., and Okamura, F.P. (1987) Crystal structures of $CaNiSi_2O_6$ and $CaCoSi_2O_6$ and some crystal-chemical relations in *C*2/*c* clinopyroxenes. American Mineralogist, 72, 375–381.

Hawthorne, F.C. and Grundy H.D. (1977) Refinement of the crystal structure of $LiScSi_2O_6$ and structural variations in alkali pyroxenes. Canadian Mineralogist, 15, 50–58.

Hazen, R.M. and Finger, L.W. (1982) Comparative Crystal Chemistry. Wiley and Sons, New York.

Hugh-Jones, D.A. and Angel, R.J. (1994) A compressional study of $MgSiO_3$ orthoenstatite up to 8.5 GPa. American Mineralogist, 79, 405–410.

Hugh-Jones, D.A., Woodland, A.B., and Angel, R.J. (1994) The structure of high-pressure *C*2/*c* ferrosilite and crystal chemistry of high-pressure *C*2/*c* pyroxenes. American Mineralogist, 79, 1032–1041.

Levien, L. and Prewitt, C.T. (1981) High-pressure structural study of diopside. American Mineralogist, 66, 315–323.

Megaw, H. (1973) Crystal Structures: A Working Approach. Saunders, Philadephia.

Morimoto, N., Nakajima, Y., Syono, Y., Akimoto, S., and Matsui, Y. (1975) Crystal-structures of pyroxene-type $ZnSiO_3$ and $ZnMgSi_2O_3$. Acta Crystallographica, B31, 1041–1049.

Ohashi, H., Fujita, T., and Osawa, T. (1982) The crystal structure of the $NaTiSi_2O_6$ pyroxene. Journal of the Japanese Association of Mineralogists, Petrologists, and Economic Geologists, 77, 305–309.

Ohashi, H., Osawa, T., and Tsukimura, K. (1987) Refinement of the structure of manganese sodium dimetasilicate. Acta Crystallographica, C43, 605–607.

Ohashi, H., Osawa, T., and Sato, A. (1990) Structures of $Na(In,Sc)Si_2O_6$ clinopyroxenes formed at 6-GPa pressure. Acta Crystallographica, B46, 742–747.

Ohashi, H., Osawa, T., and Sato, A. (1994a) $NaScSi_2O_6$. Acta Crystallographica, C50, 838–840.

——— (1994b) $NaVSi_2O_6$. Acta Crystallographica, C50, 1652–1655.

——— (1995) Low density form of $NaGaSi_2O_6$. Acta Crystallographica, C51, 2476–2477.

Origlieri, M., Downs, R.T., Thompson, R.M., Pommier, C.J.S., Denton, M.B., and Harlow, G.E. (2003) High-pressure crystal structure of kosmochlor, $NaCrSi_2O_6$ and systematics of anisotropic compression of pyroxenes. American Mineralogist, 88, 1025–1032.

Pannhorst, W. (1979) Structural relationships between pyroxenes. Neues Jahrbuch Fur Mineralogie-Abhandlungen, 135, 1–17.

——— (1981) Comparison between topological classifications of pyroxenes. Neues Jahrbuch Fur Mineralogie-Abhandlungen, 143, 1–14.

——— (1984) High temperature crystal structure refinements of low-clinoenstatite up to 700 °C. Neues Jahrbuch Fur Mineralogie Abhandlungen, 150, 270–279.

Papike, J.J. and Ross, M. (1970) Gedrites: crystal structures and intracrystalline cation distributions. American Mineralogist, 55, 1945–1972.

Papike, J.J., Prewitt, C.T., Sueno, S., and Cameron, M. (1973) Pyroxenes: comparisons of real and ideal structural topologies. Zeitschrift für Kristallographie, 138, 254–273.

Peacor, D.R. (1968) The crystal structure of $CoGeO_3$. Zeitschrift für Kristallographie, 126, 299–306.

Redhammer, G.J., Roth, G., Paulus, W., André, G., Lottermoser, W., Amthauer, G., Treutmann, W., and Koppelhuber-Bitschnau, B. (2001) The crystal and magnetic structure of Li-aegerine $LiFe^{3+}Si_2O_6$: a temperature-dependent study. Physics and Chemistry of Minerals, 28, 337–346.

Robinson, K., Gibbs, G.V., and Ribbe, P.H. (1971) Quadratic elongation: a quantitative measure of distortion in coordination polyhedra. Science, 172, 567–570.

Sato, A., Osawa, T., and Ohashi, H. (1994) $LiGaSi_2O_6$. Acta Crystallographica, C50, 487–488.

Satto, C., Millet, P., and Galy, J. (1997) Lithium vanadium metasilicate, $LiVSi_2O_6$. Acta Crystallographica, C53, 1727–1728.

Takéuchi, Y., Takamitsu, Y., Nobuhiko, H., and Masahiro, H. (1984) High-temperature crystallography of olivines and spinels. In Sunagawa, Ed., Materials Science of the Earth's Interior, p. 191–231. Terra Scientific Publishing Company, Tokyo.

Thompson, J.B. (1970) Geometrical possibilities for amphibole structures: model biopyriboles. American Mineralogist, 55, 292–293.

Thompson, R.M. and Downs, R.T. (2001) Quantifying distortion from ideal clos-

est-packing in a crystal structure with analysis and application. Acta Crystallographica, B57, 119–127.
——— (2003) Model pyroxenes I: ideal pyroxene topologies. American Mineralogist, 88, 653–666.
Tribaudino, M. (1996) High-temperature crystal chemistry of *C*2/*c* clinopyroxenes along the join $CaMgSi_2O_6$-$CaAl_2SiO_6$. European Journal of Mineralogy, 8, 273–279.
Tribaudino, M., Nestola, F., Camara, F., and Domenghetti, M.C. (2002) The high-temperature $P2_1/c$ ® $C2/c$ phase transition in Fe-free pyroxene ($Ca_{0.15}Mg_{1.85}Si_2O_6$): structural and thermodynamic behavior. American Mineralogist, 87, 648–657.
Yang, H. and Ghose, S. (1995) High temperature single crystal X-ray diffraction studies of the ortho-proto phase transition in enstatite, $Mg_2Si_2O_6$ at 1360 K. Physics and Chemistry of Minerals, 22, 300–310.
Yang, H. and Prewitt, C.T. (2000) Chain and layer silicates at high temperatures and pressures. In R.M. Hazen and R.T. Downs, Eds., Reviews in Mineralogy and Geochemistry: High-Temperature and High-Pressure Crystal Chemistry, 41. Mineralogical Society of America, Washington, D.C.
Yang, H., Finger, L.W., Conrad, P.G., Prewitt, C.T., and Hazen, R.M. (1999) A new pyroxene structure at high pressure: single-crystal X-ray and Raman study of the *Pbcn*-$P2_1cn$ phase transition in protopyroxene. American Mineralogist, 84, 245–256.
Zhang, L., Ahsbahs, H., Hafner, S., and Kutoglu, A. (1997) Single-crystal compression and crystal structure of clinopyroxene up to 10 GPa. American Mineralogist, 82, 245–258.

MANUSCRIPT RECEIVED MAY 6, 2003
MANUSCRIPT ACCEPTED SEPTEMBER 17, 2003
MANUSCRIPT HANDLED BY ALESSANDRO GUALTIERI

APPENDIX: DERIVING THE MODELS

The purpose of this section is to derive equations for the cell and positional parameters of the model *C*2/*c* pyroxene in terms of the model O atom radius, *r*, and the O3-O3-O3 angle, θ.

Octahedral edge length, $e_{M1} = e_{M1}(\theta, r) = \sqrt{8/3}\, r\sqrt{1-\cos\theta}$ (Thompson and Downs 2003).

Tetrahedral height along **a***, $h_T = h_T(r) = 2\sqrt{6}\, r/3$.

Octahedral height along **a*** is the same as the height of a tetrahedron with the same edge length, the situation found between closest-packed monolayers. Thus, $h_{M1} = h_{M1}(\theta, r) = \sqrt{6}e_{M1}/3$.

Let d = d-spacing of (1 0 0) = $a\sin\beta$. Then $d = d(\theta, r) = 2h_T + 2h_{M1}$.

The special position of M1 is used to derive expressions for β and the *z*-coordinates of some of the atoms. Inspection of hand-derived model structures with θ = 120°, 180°, and 240° reveals that M1 is always at [0 11/12 1/4] and M2 is always at [0 1/4 1/4]. There is another M1, call it M1', at [1/2 5/12 1/4]. Any point on a line drawn through these two M1 atoms has *z*-coordinate = 1/4 (Appendix Fig. 1). Thus, the projection of this line onto the **ac**-plane is parallel to **a**, and the angles it forms with **c** and **a*** are β and β – 90°, respectively. Let $g = g(\theta, r) = |[0\ 0\ z_{\mathbf{T\text{-}O2}}]^{\mathrm{t}}|$ = the length of the *z*-component of the vector from T to O2 (Appendix Fig. 2). Let $A = A(\theta, r) = -g$ when θ ≤ 180°, g when θ > 180°. The angle formed by **T-O2** and the portion of the dotted line inside the tetrahedron = 30° – (θ/2 – 60°) = 90° – θ/2, so $A = -2r\sin(90° - \theta/2)/\sqrt{3} = -2r\cos(\theta/2)/\sqrt{3}$. Let $\mathbf{M1\text{-}M1'}_c = \mathbf{M1\text{-}M1'}_c(\theta, r) = |[0\ 0\ z_{\mathbf{M1\text{-}M1'}}]^{\mathrm{t}}|$, where **M1-M1'** is the vector from M1 to M1'. Then, $\tan(\beta - 90°) = \mathbf{M1\text{-}M1'}_c/(d/2)$. From Appendix Figure 2, $\mathbf{M1\text{-}M1'}_c = 2f - g$ (since θ < 180°) = $e_{M1}/\sqrt{3} + A$, and $\beta = \beta(\theta) = 90° + \tan^{-1}[\mathbf{M1\text{-}M1'}_c/(d/2)]$.

$a = a(\theta, r) = d/\sin\beta$.

Inspection of the hand-derived models is helpful in deriving an expression for b. $b = b(\theta, r)$ = the width of one octahedral chain + one tetrahedral chain = 2 times the width of one octahedral chain = $3e_{M1}$.

$c = c(\theta, r)$ = the height of two octahedral faces = $\sqrt{3}e_{M1}$. Thus, $b/c = c/e_{M1} = \sqrt{3}$.

x-coordinates of the atoms are derived using the following relation. x = (distance from atom to **b-c** plane along a line parallel to **a**)/a = (shortest distance to **b-c** plane/d). The shortest distances are obtained by adding the heights of the appropriate number of polyhedra.

The O3 atoms are related by a **c**-glide through the origin perpendicular to **b**, allowing us to derive y_{O3}. $|[0\ y_{O3}\ 0]^{\mathrm{t}}| = r\cos(\theta/2)$, so $y_{O3} = y_{O3}(\theta) = r\cos(\theta/2)/b$.

The projection of the M1-M1' line onto the **a-c** plane is used to derive *z*-coordinates. Appendix Figure 3 shows the quantities we need to get z_T. $z_T = z_T(\theta) = 1/4 - p/c + n/c = 1/4 - m\tan(\beta - 90°)/c + (f + A)/c = 1/4 - (h_{M1}/2 + h_T/4)\tan(\beta - 90°)/c + (e_{M1}/2\sqrt{3} + A)/c$.

From Appendix Figure 4, $z_{O1} = z_{O1}(\theta) = z_T - q/c = z_T - (3/4)h_T\tan(\beta - 90°)/c$.

z_{O2} is derived in similar fashion.

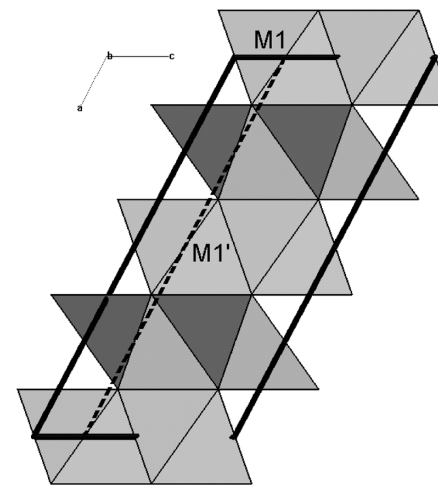

APPENDIX FIGURE 1. Polyhedral view of the unit cell of a model *C*2/*c* pyroxene looking along **b**. The special position of M1 in model *C*2/*c* pyroxene is used to derive formulae for β and the *z*-coordinates of some of the atoms as a function of model O atom radius and O3-O3-O3 angle. M1 and M1' both have *z*-coordinate of 1/4 so any point on the dotted line has *z* = 1/4. This line is used as a starting point for calculating *z*-coordinates.

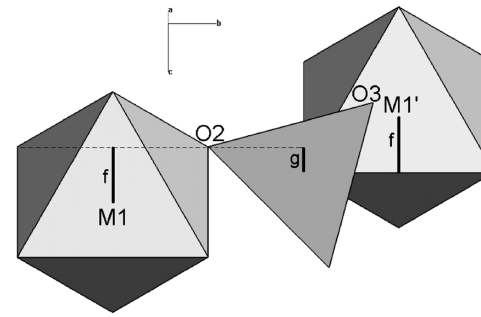

APPENDIX FIGURE 2. Polyhedral view of a portion of a model *C*2/*c* pyroxene looking along **a***. Formulae for the distances *f* and *g* are used to calculate β and *z*-coordinates for various atoms as functions of O3-O3-O3 angle. From Figure 1, $\tan(\beta - 90°) = (2f - g)$/(tetrahedral height + octahedral height).

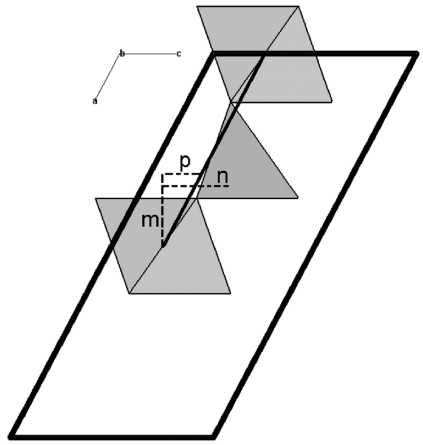

APPENDIX FIGURE 3. Polyhedral view of a portion of a model $C2/c$ pyroxene looking along **b**. Formulae for the distances p, n, and m are used to calculate z_T as a function of O3-O3-O3 angle. $z_T = 1/4 - p/c + n/c = 1/4 - m\tan(\beta - 90°)/c + n/c$.

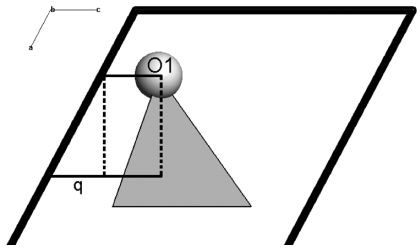

APPENDIX FIGURE 4. Polyhedral view of a portion of a model $C2/c$ pyroxene looking along **b**. Formula for the distance q is used to calculate z_{O1} as a function of O3-O3-O3 angle. $z_{O1} = z_T - q/c$. z_{O2} is derived in similar fashion.

From Appendix Figure 5, $z_{O3} = z_{O3}(\theta) = z_{O2'} + s/c = z_{O2} + 1/2 + 2r\sin(\theta/2 - 60°)/c$.

There are no atoms at special positions in $P2_1/c$ pyroxene, so a line drawn through the 2_1-screws parallel to **b** passing through [0, y, 1/4] and [1/2, y, 1/4] is used to derive β and atomic z-coordinates (Appendix Fig. 6). These two screws relate the two TA atoms and the two TB atoms in Appendix Figure 6, respectively. This placement of the axes half way between the T atoms is the key to deriving the needed distances.

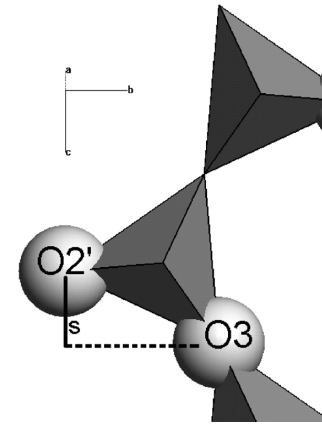

APPENDIX FIGURE 5. Polyhedral view of a portion of a model $C2/c$ pyroxene looking along **a***. Formula for the distance s is used to calculate z_{O3} as a function of O3-O3-O3 angle. $z_{O3} = z_{O2'} + s/c$.

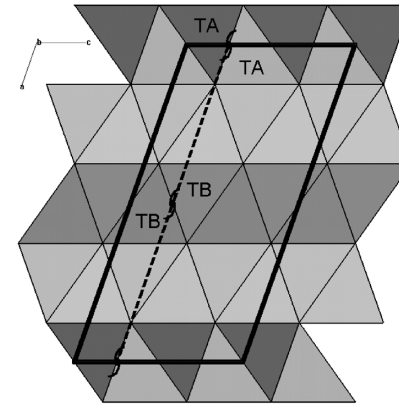

APPENDIX FIGURE 6. Polyhedral view of the unit cell of a model low clinopyroxene looking along **b**. No atoms are on special positions in low clinopyroxene, so 2_1-screws are used to define $z = 1/4$ line.

Data for the different models are given in Appendix Table 1.

APPENDIX TABLE 1. Exact crystal structures of four model pyroxenes

	$C2/c$ model pyroxene with fully extended chains	$P2_1/c$ model pyroxene with fully extended A-chains and fully rotated B-chains	$Pbca$ model pyroxene with fully extended A-chains and fully rotated B-chains	$Pbcn$ model pyroxene with fully extended chains
θ	180°			180°
θA		180°	180°	
θB		120°	120°	
a	$\sqrt{(288 + 128\sqrt{3})}\, r/3$	$\sqrt{[(116 + 32\sqrt{3})/3]}\, r/3$	$(4\sqrt{6} + 24\sqrt{2})r/3$	$(4\sqrt{6} + 8\sqrt{2})r/3$
b	$4\sqrt{3}\, r$	$4\sqrt{3}r$	$4\sqrt{3}\, r$	$4\sqrt{3}\, r$
c	$4r$	$4r$	$4r$	$4r$
β	$\cos^{-1}(-2c/3a)$	$180 - \tan^{-1}((\sqrt{6} + 6\sqrt{2})/3)$		
T	$[(2\sqrt{3} - 1)/8, 1/12, 1/(2\sqrt{3})]$			$[(2\sqrt{3} - 1)/8, 1/12, 1/12]$
TA		$[(2\sqrt{3} - 1)/44, 1/3, (21 + 2\sqrt{3})/88]$	$[(21 + 2\sqrt{3})/88, 1/3, 0]$	
TB		$[(39 - \sqrt{3})/66, 5/6, (28 - \sqrt{3})/132]$	$[(60 + \sqrt{3})/132, 1/3, 5/6]$	
M1	[0, 11/12, 1/4]	$[(9 + 4\sqrt{3})/66, 2/3, (5 + \sqrt{3})/33]$	$[(21 + 2\sqrt{3})/66, 2/3, 5/6]$	[0, 1/12, 3/4]
M2	[0, 1/4, 1/4]	$[x_{M1}, 0, z_{M1}]$	$[x_{M1}, 1/2, z_{M1} - 1/2]$	$[x_{M1}, 1/4, z_{M1} - 1/2]$
O1	$[1 - \sqrt{3}/2, 1/12, 3/4 - 1/\sqrt{3}]$			$[(2 - \sqrt{3})/2, 1/12, 1/12]$
O1A		$[(23 - 2\sqrt{3})/22, 1/3, (6 - \sqrt{3})/22]$	$[(6 - \sqrt{3})/22, 1/3, 0]$	
O1B		$[(2/3)z_{O3A}, 5/6, z_{O2A}/3]$	$[(39 - \sqrt{3})/66, 1/3, 5/6]$	
O2	$[(\sqrt{3} - 1)/2, 1/4, 1/\sqrt{3} - 1/4]$			$[(\sqrt{3} - 1)/2, 1/4, 1/12]$
O2A		$[2x_{TA}, 1/2, (3/2)z_{M1}]$	$[(5 + \sqrt{3})/22, 1/2, 0]$	
O2B		$[(45 - 2\sqrt{3})/66, 0, 2z_{TB}]$	$[(27 + \sqrt{3})/66, 1/2, 2/3]$	
O3	$[x_{O2}, 0, z_{O2} - 1/4]$			$[x_{O2A}, 0, 1/3]$
O3A		$[x_{O2A}, 1/4, 2z_{TA}]$	$[x_{O2A}, 1/4, 3/4]$	
O3B		$[x_{O2B}, 2/3, 2z_{O2B}]$	$[x_{O2B}, 1/6, 2/3]$	